CM² MAGAZINE

第 21 期

南方科技大学海洋磁学中心主编

创刊词

海洋是生命的摇篮，是文明的纽带。地球上最早的生命诞生于海洋，海洋里的生命最终进化成了人类，人类的文化融合又通过海洋得以实现。人因海而兴。

人类对海洋的探索从未停止。从远古时代美丽的神话传说，到麦哲伦的全球航行，再到现代对大洋的科学钻探计划，海洋逐渐从人类敬畏崇拜幻想的精神寄托演变成可以开发利用与科学研究的客观存在。其中，上个世纪与太空探索同步发展的大洋科学钻探计划将人类对海洋的认知推向了崭新的纬度：深海（deep sea）与深时（deep time）。大洋钻探计划让人类知道，奔流不息的大海之下，埋藏的却是亿万年的地球历史。它们记录了地球板块的运动，从而使板块构造学说得到证实；它们记录了地球环境的演变，从而让古海洋学方兴未艾。

在探索海洋的悠久历史中，从大航海时代的导航，到大洋钻探计划中不可或缺的磁性地层学，磁学发挥了不可替代的作用。这不是偶然，因为从微观到宏观，磁性是最基本的物理属性之一，可以说，万物皆有磁性。基于课题组的学科背景和对海洋的理解，我们对海洋的探索以磁学为主要手段，海洋磁学中心因此而生。

海洋磁学中心，简称 CM^2，一为其全名“Centre for Marine Magnetism”的缩写，另者恰与爱因斯坦著名的质能方程 $E = MC^2$ 对称，借以表达我们对科学巨匠的敬仰和对科学的不懈追求。

然而科学从来不是单打独斗的产物。我们以磁学为研究海洋的主攻利器，但绝不仅限于磁学。凡与磁学相关的领域均是我们关注的重点。为了跟踪反映国内外地球科学特别是与磁学有关的地球科学领域的最新研究进展，海洋磁学中心特地主办 CM^2 Magazine，以期与各位地球科学工作者相互交流学习、合作共进！

“海洋孕育了生命，联通了世界，促进了发展”。 21 世纪是海洋科学的时代，由陆向海，让我们携手迈进中国海洋科学的黄金时代

目 录

建安二十四年·关羽

葛坤朋

东华理工大学地球物理与测控技术学院

建安二十四年五月，汉中争夺战以刘备惨胜告终，曹操携军迁民退出汉中，刘备至此全据益州。

但曹操只是兵退长安，未回许都。七月，刘备进位汉中王，曹操仍在长安，有以僭位为名，继续征伐刘备的计划。刘备深以为恐，与群臣商议后，命前将军、襄阳太守、汉寿亭侯关羽北伐襄樊，牵制曹军，力图迫使曹操退出长安，缓解益州之危。

快马送信至荆州江陵城内，关平看信后禀报关羽。

关平：父亲，伯父命您北伐襄樊。我看曹贼虽然丢了汉中，但只是兵退长安，其意仍未放弃汉中。因此伯父命您此时北伐襄樊，是解汉中之危。

关羽：好吧，传令荆州各部，整顿水陆军马，择日北伐襄樊。

关平：父亲，去年伯父跟曹操会战，侯因等人在宛城反叛曹贼，宛洛震动响应您，彼时天赐良机，也未见您行动啊？

关羽：汝实不知，我虽能随时兴兵，无奈东吴虎视眈眈，绝无汉心，我怎能安心北伐？如今，你伯父与我，既是兄弟，又是君臣。今汉中王亲令我北伐，我安能不听令？

关平：荆州兵两次分兵入川，所剩兵力有限。况且还要防备孙权，能北伐的兵力实在有限。父亲您是怎么想的？

关羽：曹贼新败，各地叛乱，此时北伐兴汉并无不妥。但其自行退出汉中，并迁出居民，实力未损。如我在北伐中交战无胜机可取，当立即撤退。毕竟以荆州三郡之力攻襄樊四战之地，如孙权之攻合肥，不利居多。

关平：但与魏军战端一开，不是我们想停就能停的。彼时益州绝远，援军一时难至，如之奈何？

关羽：可退回荆州，或经夷道退回蜀中。另外我还有孟达军出秭归攻上庸，

可做援军。再不济，也可为接应。我军至少可以入汉中，全身而退。

关平：如果父亲被曹贼援军反包围呢？

关羽：我自有陆军联络，水军占据汉水，进退有据。

关平：那如果吴军背后偷袭呢？

关羽：我军北伐兴汉，师出有名。吴军无故偷袭，千古不齿。但这些春秋褒贬之义他们听不懂。我已经沿湘水长江设立烽火联营，况且江陵守军为我兄亲信，短日内御敌当无虞。待我援军返回，可解荆州之围。

关平：父亲没有想过万一吗？万一曹贼起倾国之兵援助襄樊，反包围我军；孙权起倾国之兵偷袭荆州，断我入川归路；而上庸又不发援兵，甚至不做接应呢？

关羽：哈哈，彼时我手中仍有青龙偃月刀，胯下仍有赤兔追风马，来去自如，飘然往返，彼能奈我何？

关平陷入沉思。

关羽：平儿，那是笑话。战局不利的情况有三种。其一是战败后如果能安全退回荆州，依赖军实天险，将来还可整顿军马一战；更坏的情况，如果荆州丢了，或可借兵汉中再图荆襄；最坏的情况，是全世界与我们为敌，那样的话我们恐怕要死无葬身之地了。不过那一天如果真的到来，或许大汉的运势已非我关某所能挽回了。我必把赤兔马和偃月刀让与你，你还年轻，跟着孔明未来不可限量。而你看看父亲，年届六旬，戎马四十年，须发皆已斑白。如果能死在沙场之中，死在未倾的大汉穹隆之下，不也是美事一桩吗？这也是求仁得仁，了无遗憾呀。

关平哭道：不，父亲，不会那样的，我们一定能赢。如果真的到了那一刻，我愿意陪您一起死！

关羽朗声大笑。

关平：那父亲，关于北伐，除了受命之外，您自己是怎么想的呢？

关羽：这还得提提以前的事情。跟着你伯父去隆中拜访孔明的时候，听那个二十多岁的小伙子讲北伐大计，说什么“待天下有变，则命一上将出荆州以向宛洛，将军自帅大军出秦川，则天下可定”。说的或许就是现在，也或许是等曹贼死去。但际遇也许稍纵即逝，况且我已经年近六旬，孔明也已经快四十了，没时间再等了。若不然，等我们这些老家伙逝去，谁还肯会为大汉卖命呢？看看东吴那份吃相，还不明白吗？

关平：父亲，您想过没有。如果曹操称帝怎么办？如果伯父也称帝了怎么办？我们到底该忠于谁呢？您这个襄阳太守，汉寿亭侯是当朝孝献皇帝封赏的呀。

关羽：曹贼称帝，我必定北伐诛贼。你伯父称帝，那也是延续大汉血脉，当朝开国皇帝光武帝不也如此吗？

关平：父亲，如果汉室未亡，而伯父却称帝，怎么办？您真的觉得伯父是忠于朝廷的吗？

关羽沉默。

关平：父亲，伯父之所以百分之百信任您，是因为您对国家之忠，对兄长之义是一体的。如果哪一天这忠义不能两全呢？

关羽笑了：哈哈，我儿可教。这才说中了我北伐的根本原因啊。你伯父的心大，我不敢妄加猜测。我是一介臣子，能靠际遇和努力获封大汉“襄阳太守，汉寿亭侯”的爵位已经心满意足啦，如今又获得兄长汉中王封赏的“前将军，假节钺”，更是诚惶诚恐。此番北伐，实为孤军奇谋。成则全据荆益天险，进逼宛洛，他日我兄为再生周公，我则忠义两全；败则天下三分，我兄续汉基业，我慷慨赴死，也得忠义。这正是我的私心啊。兄长此时让我北伐，也是对我的成全呀。若是期年之后，时局难测。

关羽继续：我想你伯父也应知道我的心思。我们都是六旬老翁了，而曹贼却阳寿未尽，天下之变在何时未知。我虽是身无背景的亡命之人，但却知春秋之义。跟从你伯父，感激知遇之恩，义重如山；后来被曹贼所围，不肯为其所用，但为报不杀之恩，官渡斩颜良，解白马后继续投奔你伯父；荆州守江夏，治水军；赤壁绝北道，围江陵；始终深得你伯父信任，所以才能驻守荆州十年。

关平：嗯，父亲人生大起大落，不忘忠义，不愧为盖世英雄！

关羽：驻守荆州此间，我听从孔明先生的建议，未曾与孙权生隙，更未曾交兵。但殊不知人性千年不变，喜欢以成败论英雄，此番若是战局不利，只怕后世多半要给我一个骄傲辱吴的浮夸名声。不过能以我的“前车之鉴”，警醒后人发扬谦卑清醒的品质，也不失为一件好事啊。

关平：嗯嗯，那您没想过，想办法保全荆州，跨有荆益，做长久的恢复汉室的计划吗？

关羽：兄长命我北伐襄樊，汉中却未动，想必是元气未复，怕曹贼继续进攻。

因为曹贼虽败，但实力仍然强大。再者，如果只图偏安，无法歼灭敌人有生力量，跨有荆益也无用处。如同东吴一般，纵有三州之地也是坐等灭亡耳。对于我这老翁，机不可失，时不再来。后面的际遇，要多拜托孔明先生了。回去收拾行装吧，计日北伐。

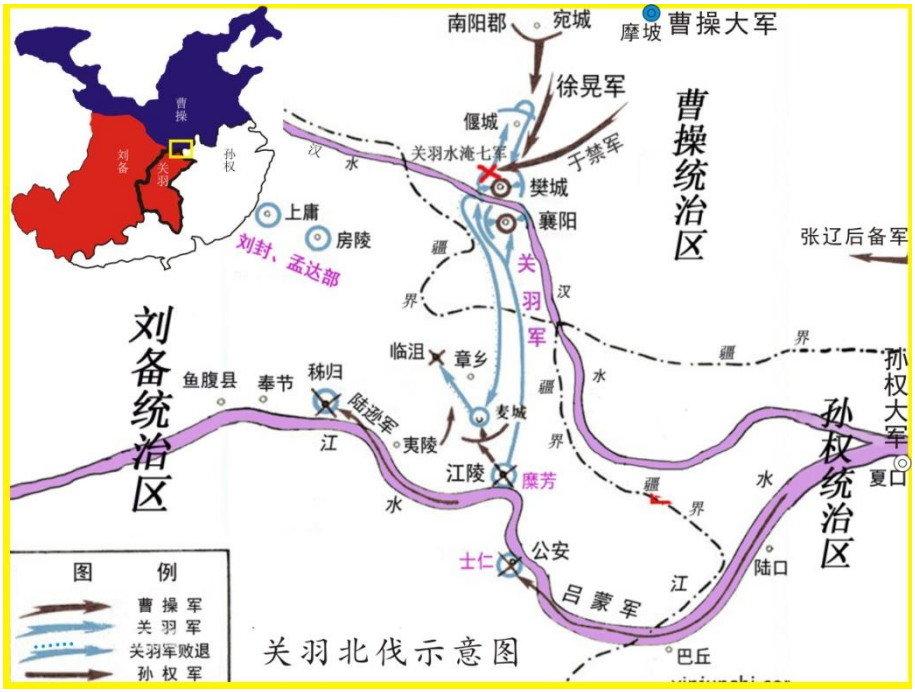

建安二十四年七月关羽受命北伐；八月淹七军，擒于禁，斩庞德，威震华夏；九月拔房陵，围襄阳、困樊城，迫降荆州刺史，曹操议迁都；而后司马懿谏止，魏起倾国之兵相救，曹操撤出长安，大军至豫州摩坡，并暗说孙权出战偷袭；孙权即起倾国之兵袭荆，陆逊攻秭归断夷道，吕蒙攻江陵、公安，孙权大军至江夏；然后至始至终，刘备诸葛亮未发一兵一卒，上庸刘封孟达未做任何接济。闰十月樊城解围，荆州被袭取，十一月关羽走麦城，十二月兵败被俘。

事实是关羽孤军面对曹操、司马懿、徐晃、张辽、于禁、曹仁、庞德，孙权、吕蒙、陆逊、诸葛瑾、潘璋、丁奉以及两军背后的几十万人马。

建安二十四年十二月，关羽亡，关平亡；一个月后，曹操亡；十个月后，大汉亡。

于是有：

一代英雄，二尺美髯。

三分天下，实第四极。

五虎上将，六旬北伐。

水淹七军，威震八方，

九州祭拜，十全武功。

评语：在后赤壁、前三国时代，天下其实有四路诸侯。曹、孙、刘和关，只不过关羽始终忠于刘备（或者汉室），如果刘备和汉室分道扬镳，关羽的地位就会非常尴尬，也会凸显出其第四路诸侯的模样。设想关羽北伐期间，如果孙权不去偷袭，而是在合肥拖住魏军，关羽拿下襄樊，擒杀曹仁。虽然曹操一时难以被拿下，但不多年曹操死后，则“天下有变”的真正时机到来。彼时刘关孙三路军北伐，天下可定。刘备做周公，关羽做召公，孙权做太公，三公辅汉，剧本完美。无奈，孙权就是一堆散沙里面最聪明的那一粒沙，最后拉着蜀汉一起坐等灭亡，成全了魏晋。本来命运在自己手里，可以把自己的枭雄称号变成英雄。结果呢？结果只有关羽做了英雄（真心英雄）。曹、孙、刘全部都成了广义英雄（英武的枭雄），其实还是枭雄。

关羽之没，打醒了刘备，最后的老炮儿发动了夷陵之战，爆发了最后的一点痞子英雄气。也点醒了诸葛，时刻不忘兴复汉室，还于旧都的春秋之义。

第 11 章　磁滞回线—SD 颗粒

对于铁磁性物质，其初始磁化强度(M)为零，在外场(H)激发下会发生磁化现象。当场足够大时，其磁化强度达到饱和(Saturation magnetization, M_s)。使得磁化强度达到饱和时的临界场称之为饱和场(H_{sat})。此时逐渐减小外场，M 并不沿着初始的磁化曲线减小，而是滞后于外场的变化，称之为磁滞(hysteresis)现象。如果让外场在+H 和-H 之间做周期性变化，M-H 曲线就是一条闭合的曲线，称之为磁滞回线(Hysteresis loop)。

与磁滞现象相对应的叫做非磁滞现象（Unhysteresis），也就是场可以加得很大，场去掉，M = 0。看起来，顺磁性物质就具有典型的非磁滞行为。SP 颗粒也具有这种性质。

由于 M 和 H 不同步变化，当 H = 0 时，M 却不为零，这个遗留的磁化强度叫做剩磁 M_r。正是因为有剩磁的存在，磁性颗粒在地磁场磁化后，保留和当时地磁场相关的信息。如果磁性颗粒都是顺磁或超顺磁行为，肯定无法进行古地磁研究了。

通过磁滞回线的测量，可以得到诸多磁性参数，包括饱和磁化强度 M_s、剩余磁化强度(M_{rs})、矫顽力(H_c 或者 B_c)、初始磁化率、和高场顺磁磁化率等。磁滞回线的形态与磁性颗粒的磁畴状态和矿物类型等密切相关。

我们先看最简单的 SD 颗粒的磁滞回线。

对于拉长型的 SD 颗粒，其长轴就是易磁化轴。我们沿着长轴来加场，让 M 平行于长轴，此时就是饱和状态（M_s），因为 M 不会随着 H 增大而增大。由于

有 H_K 的影响，我们逐渐减小 H 到零，M 还会保持其饱和状态，所以此时的剩磁与 Ms 相等：$M_{rs} = M_s$。

然后我们反向加场，直到 $H = -H_K$ 时，M 就会 180°反向排列，达到反向饱和状态。之后我们再正向加场，当 $H = H_K$ 时，M 又会 180°偏转回正向状态，从而整体形成一个矩形回路。

这种矩形的磁滞回线并不多见，如果碰到了，就说明磁性颗粒很可能真的是排列得很好的拉长型 SD 颗粒。而且加场方向应该平行于它们的长轴方向。

垂直方向的短轴是难磁化轴，也就是说 M 在这个方向不容易维持，如果没有外场，受到能量最小化原理控制，M 就会偏转向易磁化轴，从而在短轴方向的 M 分量为零。所以，我们看到的所谓磁滞回线就显得非常单薄。实际上就是没有磁滞行为，剩磁也为零。

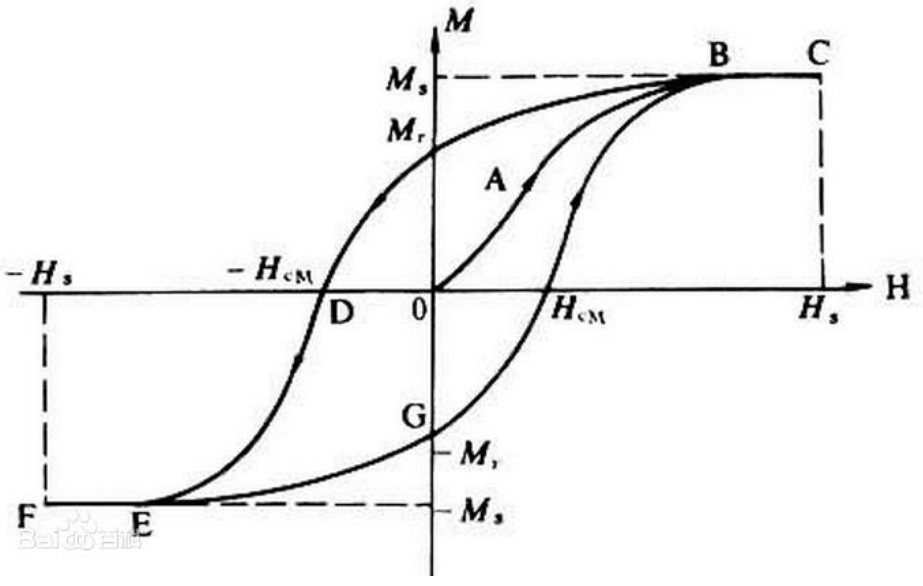

图 1 自然样品的典型磁滞回线。

如果有很多拉长型的 SD 颗粒，它们的长轴在空间中随机分布，这时候，我们通过空间积分的方式得到上图的这种典型的磁滞回线。此时，$M_r = 0.5 * M_s$，

$H_C = 0.5 * H_K$。

现在我们遇到了三种情况都没有剩磁：顺磁物质、超顺磁物质、以及沿着拉长型 SD 颗粒的短轴磁化。这三种情况下，对应的矫顽力为零 $H_c = 0$。

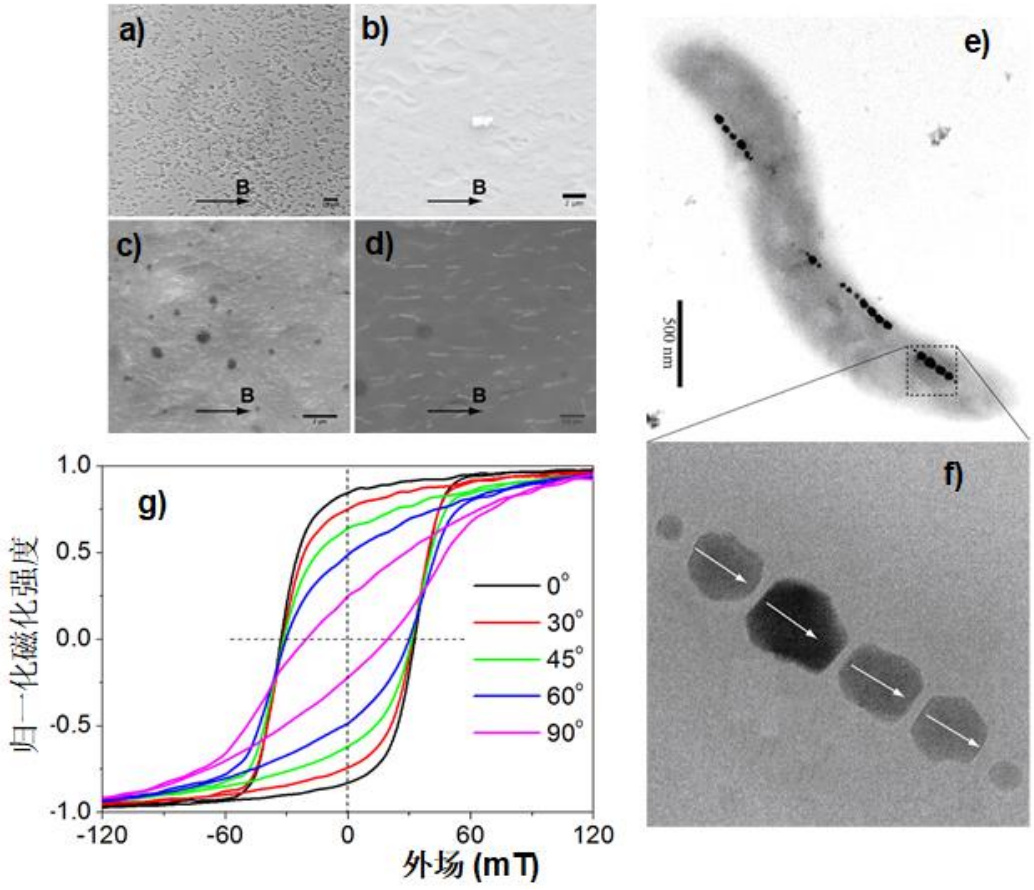

图 2　a)-d) 定向排列的磁细菌；e) 单个磁细菌形态；f) 磁细菌内定向排列的磁小体；g) 沿着定向排列的磁细菌不同方向测量的磁滞回线。a-d) 中的箭头指向外场方向，f)中的箭头指向磁小体的磁化强度方向；g)中的度数为测量方向与定向排列方向的夹角。

上图展示了一组沿着定向排列磁细菌不同方向测量的磁滞回线。磁细菌体内含有成链状分布的纳米级磁小体（磁铁矿）。整体上，这些链状分布的磁小体等效于一个拉长状具有单轴各向异性的 SD 磁铁矿。磁小体的排列方向就是其易磁化轴方向。在外场作用下，这些磁细菌会定向排列，从而整个样品具有明显的各

向异性特征。平行于磁细菌的排列方向，其磁滞回线类似于一个矩形，具有最大的矫顽力。在垂直方向，其矫顽力最小。

实测的定向排列磁小体磁滞回线与真正的矩形磁滞回线还存在着差别，这种差别主要来源于磁细菌的非完全定向排列。即使如此，该研究能够反应出具有单轴各向异性(uniaxial single domain, USD)颗粒，在不同测量方向上磁滞回线的特征。

除了磁化率，矫顽力也和颗粒的大小密切相关。

SP 颗粒的矫顽力为零，SD 颗粒的矫顽力最高。对于球形的 SD 磁铁矿颗粒，其矫顽力约为 20 mT，拉长型的 SD 颗粒，其矫顽力> 20 mT。跨越 SD 颗粒后，磁畴状态逐渐向涡旋状态及 PSD/MD 转化，矫顽力会随着粒径的增大逐渐减小到几个 mT。

可见，矫顽力这个参数也可以被用来研究磁畴状态，进而推断磁性颗粒的大小。比如们研究一个剖面，从上往下，样品的矫顽力逐渐减小，这到底代表着什么？

首先我们必须要判断 SP 颗粒是否存在显著影响。可以通过测量频率磁化率，以及 CBD 处理等方式达到这一目的。如果发现 SP 颗粒影响不明显，那么就符合矫顽力减小，磁性颗粒的粒径会增大这个规律。如果 SP 颗粒含量很多，就属于 SD+SP 的组合模式，SP 含量越高，矫顽力也就越低。

自然界中经常会是几种磁性矿物的组合，最为典型的就是高矫顽力和低矫顽力矿物组合，这种组合方式会产生一种叫做细腰型（Wasp-waist shape）的磁滞回线。比如 SP+SD 组合、磁铁矿和赤铁矿的组合等等。

这是因为当具有不同矫顽力的磁性矿物混合时，在低场和高场，这些矿物

的贡献不一致。比如，在低场，SP 和 MD 颗粒对场的变化反应敏感，而在高场，SD 的贡献会逐渐加强，整体造成细腰形的磁滞回线。

矫顽力的不同即可以由粒径变化引起，也可以由矿物种类的变化引起。一般来说，反铁磁性矿物的矫顽力比铁磁性的要大。因此，当混合赤铁矿和磁铁矿时，也会造成细腰型的磁滞回线。值得注意的是，和 SP+SP 磁铁矿混合颗粒相比，赤铁矿和磁铁矿的混合颗粒具有更高的矫顽力。

文献导读

1. 晚上新世到早更新世青藏高原东北部显著的冰期-间冰期气候变化的沉积学记录

翻译人：仲义 zhongy@sustech.edu.cn

Yin Lu, Nico Dewald, Andreas Koutsodendris et al., ***Sedimentological evidence for pronounced glacial-interglacial climatic fluctuations in NE Tibet in the latest Pliocene to early Pleistocene.*** *[J]. Paleoceanography and Paleoclimatology, 2020.*

摘要：北半球冰期增强和青藏高原的隆升被认为是驱动上-更新世以来中纬度中亚地区气候变化的主要驱动因素。而大多数用来证明这一假说的记录都在青藏高原外部区域（例如中国黄土地区），缺少这一时期在青藏高原内部的古气候记录。因此，本文利用青藏高原东北部柴达木盆地的沉积记录（500 年分辨率），结果显示出在 2.7Ma 到 2.1 Ma 之间呈现明显的冰期-间冰期的气候变化。冰期主要表现为较粗的粒度、较少的有机质含量及碳酸盐含量最高，反之间冰期呈现相反趋势。对比地球轨道参数及中国黄土记录指标显示该记录主要受控于北半球冰盖增强导致的西伯利亚高原和东亚冬季风系统的改变。同时进一步证实了青藏高原的地形对西风带的强度和位置具有重要影响。

ABSTRACT: The intensification of Northern Hemisphere glaciation (iNHG) and uplift of the Tibetan Plateau have been argued to be among the main drivers of climate change in mid-latitude Central Asia during the Plio-/Pleistocene. While most proxy records that support this hypothesis are from regions outside the Tibetan Plateau (such as from the Chinese Loess Plateau), detailed paleoclimatic information for the plateau itself during that time has yet remained elusive. Here we present a temporally highly resolved (~500 years) sedimentological record from the Qaidam Basin situated on the northeastern Tibetan Plateau that shows pronounced glacial-interglacial climate variability during the interval from 2.7 to 2.1 Ma. Glacial (interglacial) intervals are generally characterized by coarser (finer) grain-size, minima (maxima) in organic-matter content, and maxima (minima) in carbonate content. Comparison of our results with Earth's orbital parameters and proxy records from the Chinese Loess Plateau suggests that the observed climate fluctuations

were mainly driven by changes in the Siberian High/East Asian winter monsoon system as a response to the iNHG. They are further proposed to be enhanced by the topography of the Tibetan Plateau and its impact on the position and intensity of the westerlies.

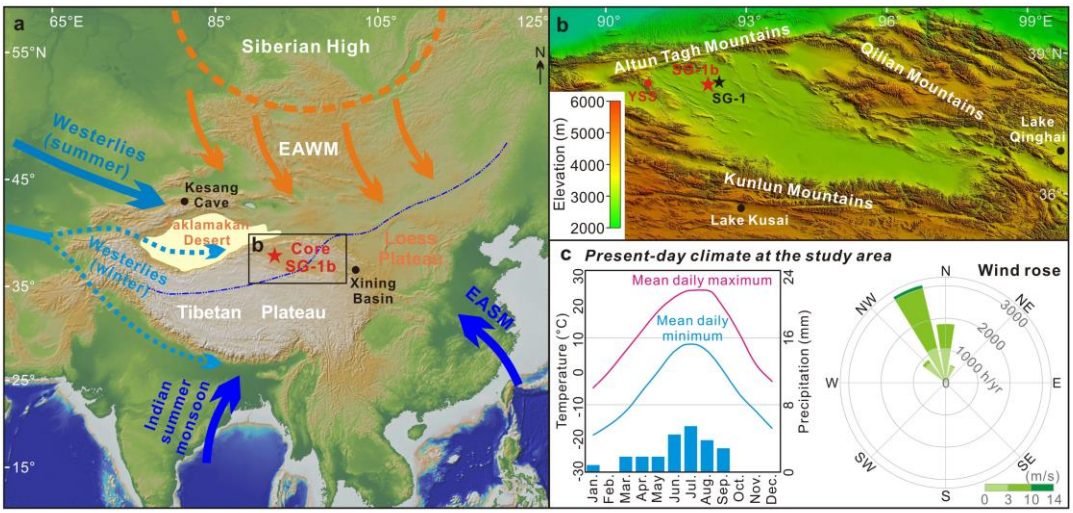

Figure 1. Geological setting and atmospheric circulation pattern of the study region. (a) Atmospheric circulation pattern of the study region; EAWM = East Asian winter monsoon; EASM = East Asian summer monsoon; the dashed blue line indicates the limit of modern Asian summer monsoon influence (Gao et al., 1962). (b) Core location (red star) and topography of the Qaidam Basin and surrounding area. (c) Present-day climate of the study area (adopted from: https://www.meteoblue.com/en/weather/forecast/modelclimate); the meteorological data are simulated based on observed weather data of observational stations in the west and east of the drilling site. The black points and star in panels (a) and (b) indicate localities referred to in the text; YSS, Youshashan, where modern eolian deposits have been collected.

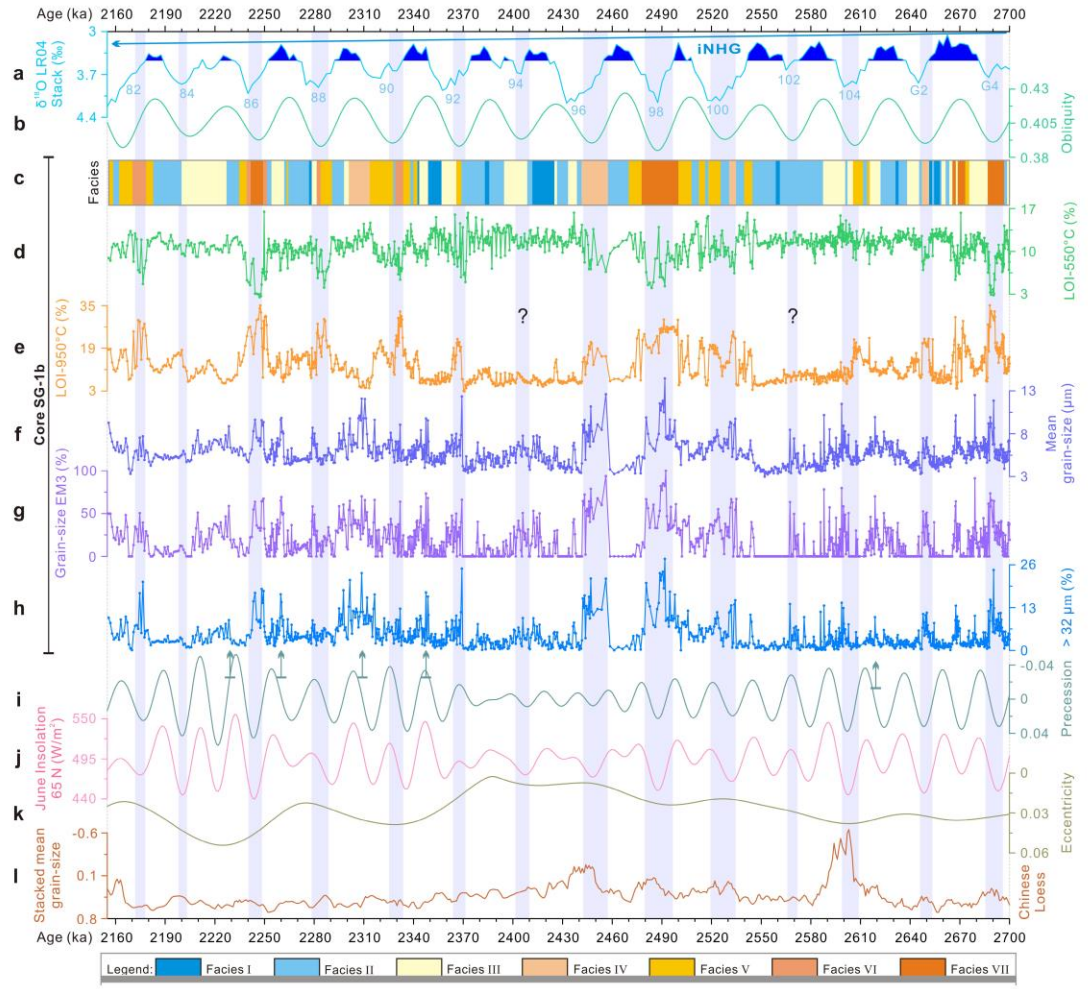

Figure 2. Comparison of proxy records from Core SG-1b, western Qaidam Basin (c-g) plotted against the global benthic foraminiferal δ18O stack (a), orbital parameters (b, i, j, k) and grain-size from the Chinese Loess Plateau (l). (a) The LR04 stack for the interval between MIS G4 and 82 (Lisiecki and Raymo, 2005); iNHG = intensification of Northern Hemisphere glaciation. (b) Orbital obliquity from the La2004 solution (Laskar et al., 2004). (c) Facies distribution of Core SG-1b. (d) Loss on ignition (LOI) of sediments at 550 ℃ (indicating organic-matter content) in Core SG-1b. (e) LOI-950 ℃ (indicating carbonate content) in Core SG-1b. (f) Mean grain-size of sediments in Core SG-1b. (g) Content of grain-size EM3 in Core SG-1b. (h) Content of coarse silt and fine sand in Core SG-1b. (i), (j) and (k) orbital precession (light green) from the La2004 solution, summer insolation (pink) and eccentricity (gray) (Laskar et al., 2004); the light green arrows indicate grain-size coarsening within interglacials, corresponding to strengthened East Asian summer monsoon (EASM) precipitation. (l) Stacked loess mean grain-size from the Chinese Loess Plateau (Sun et al., 2006). The "?" indicates weakly expressed glacials in the Core SG-1b record.

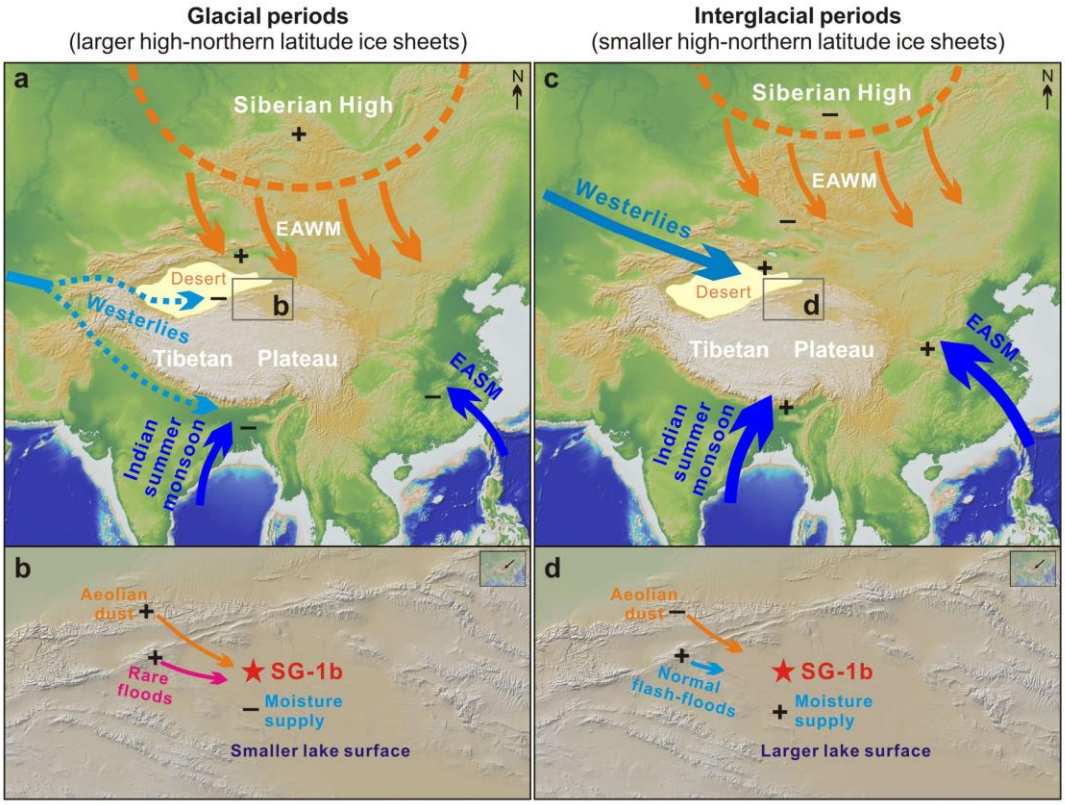

Figure 3. Schematic model illustration of the proposed forcing of the glacial-interglacial climate fluctuations recorded in Core SG-1b sediments during the latest. Pliocene to early Pleistocene. The "+" and "-" refer to the enhancement and reduction of a target process, respectively.

2. 俯冲过程中大洋板片顶部熔融：对微量元素循环和埃达克岩成因的指示

翻译人：冯婉仪 fengwy@sustech.edu.cn

Hernández-Uribe D, Hernández-Montenegro J D, Cone K A, Palin R M. ***Oceanic slab-top melting during subduction: Implications for trace-element recycling and adakite petrogenesis****[J]*. ***Geology****, 2020, 48: 216-220.*

摘要：洋壳在俯冲过程中的脱挥发分作用控制了弧火山作用和微量元素循环。俯冲过程中释放的流体类型（富水流体或含水熔体）受控于俯冲带的热结构。最近的热力学模型和实验岩石学的结果表明，几乎在所有的俯冲带中都可以发生板片熔融，尽管这并没有完全得到岩石记录的支持。在这里，我们通过相平衡模型表明，即使在水饱和的情况下，无论是新鲜的还是热液蚀变的玄武岩在俯冲过程中也很少发生熔融。熔融作用只在俯冲板片顶部最高温的地热区发生，富水流体在弧前区域被释放，深熔作用只局限在弧下深度，这导致高 SiO_2 的埃达克质岩浆作用发生。我们假设富水流体和含水熔体会在“热”俯冲带中提高化学循环效率。我们的模型显示，俯冲的热液蚀变玄武岩比原始的玄武质地壳更肥沃，它会使俯冲过程中流体和熔体的产量提高，并导致更大程度的化学循环。在这篇文章中，我们提出了一个岩石学模型来解释洋壳俯冲过程中熔融现象（的缺乏），并指出许多大规模的地球表面和内部的质量传递模型可能需要修正。

ABSTRACT: Arc volcanism and trace-element recycling are controlled by the devolatilization of oceanic crust during subduction. The type of fluid—either aqueous fluids or hydrous melts—released during subduction is controlled by the thermal structure of the subduction zone. Recent thermomechanical models and results from experimental petrology argue that slab melting occurs in almost all subduction zones, although this is not completely supported by the rock record. Here we show via phase equilibrium modeling that melting of either fresh or hydrothermally altered basalt rarely occurs during subduction, even at water-saturated conditions. Melting occurs only along the hottest slab-top geotherms, with aqueous fluids being released in the forearc region and anatexis restricted to subarc depths, leading to high-SiO_2 adakitic magmatism. We posit that aqueous fluids and hydrous melts preferentially enhance chemical recycling in “hot” subduction zones. Our models show that subducted hydrothermally altered basalt is more fertile than pristine basaltic crust, enhancing fluid and melt production during subduction and leading to a greater

degree of chemical recycling. In this contribution, we put forward a petrological model to explain (the lack of) melting during the subduction of oceanic crust and suggest that many large-scale models of mass transfer between Earth's surface and interior may require revision.

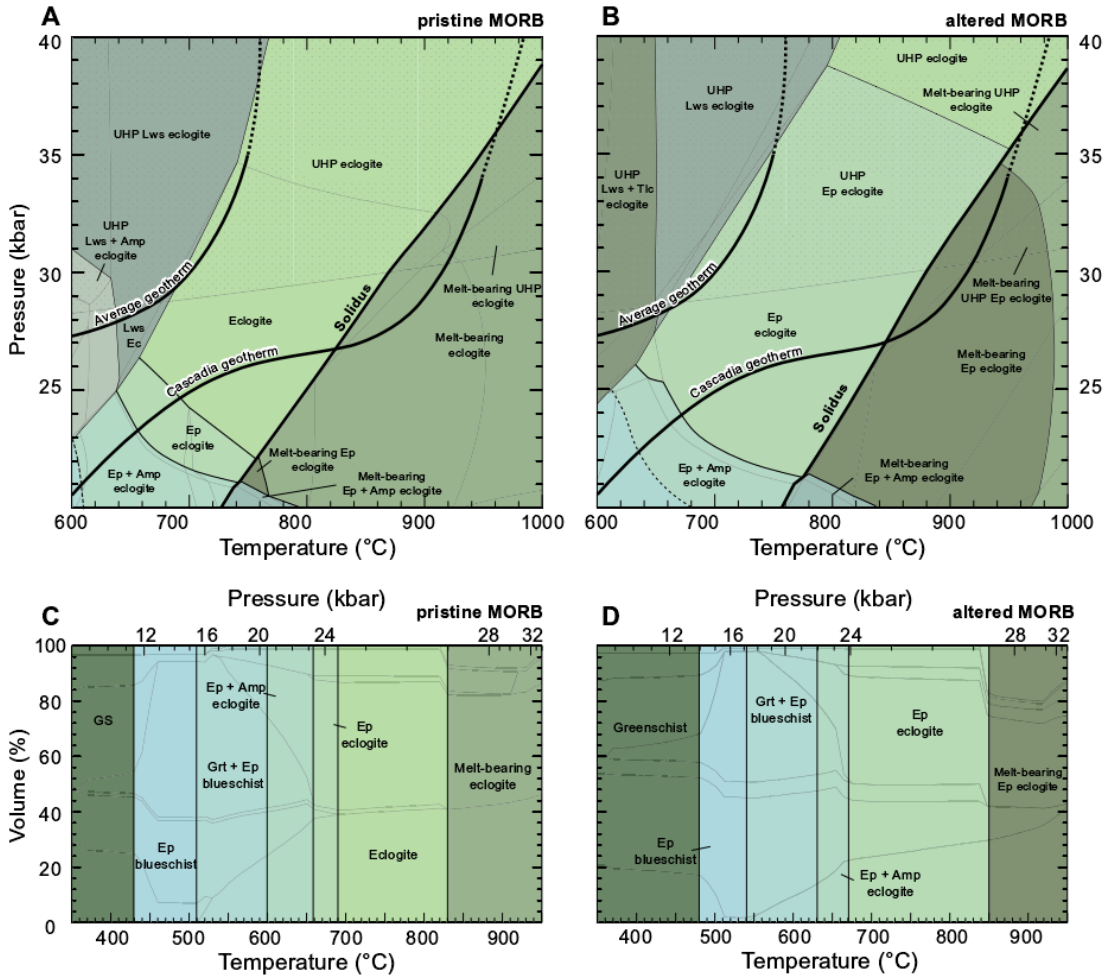

Figure 1. Petrological models for subducted uppermost basaltic portion of oceanic crust. (A, B) Pressure-temperature (P-T) summary phase equilibrium diagram showing metamorphic subfacies for pristine (A) and altered (B) mid-oceanic ridge basalt (MORB) compositions. Detailed P-T phase equilibrium models are shown in Figure DR4 in the Data Repository (see footnote 1). Modeled P-T geotherms are shown as solid thick lines (dashed lines are extensions of geotherms, where modeling was not performed). The geotherms are from Syracuse et al. (2010); see text for details. Stippled area corresponds to ultrahigh-P (UHP) conditions. (C, D) Calculated phase assemblages along a hot geotherm showing corresponding metamorphic subfacies for pristine (C) and altered (D) MORB compositions. Gray lines underlying the metamorphic subfacies fields are cumulative mineral proportions (see Figure DR2 for details). The earlier part of P-T evolution shown in C and D is not shown in B. The term "blueschist" was assigned to lithologies with volume proportions of Amp + Ep/Lws > Grt + Omp, and "eclogite" to those with the inverse relationship. Details of modeled proportions are shown in Figure DR2. Amp-amphibole; Ep-epidote; Lws-lawsonite; Tlc-talc; Grt-garnet; Omp-omphacite; Ec-eclogite; GS-greenschist.

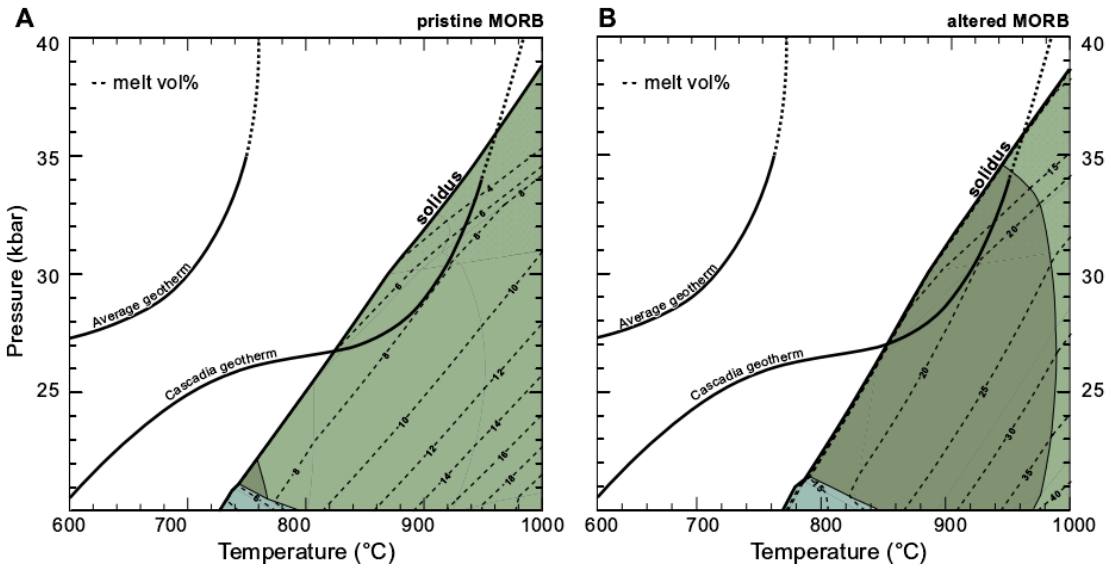

Figure 2. Calculated melt proportion at suprasolidus conditions for pristine (A) and altered (B) mid-oceanic ridge basalt (MORB). Modeled pressure-temperature (P-T) geotherms are shown as solid thick lines (dashed lines are extensions of geotherms, where modeling was not performed). Stippled area corresponds to ultrahigh-P conditions. The geotherms are from Syracuse et al. (2010); see text for details. Shaded regions correspond to the same as shown in Figures 1A and 1B.

3. 北印度洋过去 4 Ma 风尘的变化—来自粗粉尘颗粒的证据

翻译人：蒋晓东 jiangxd@sustech.edu.cn

Lindhorst, S., Betzler, C., & Kroon, D. 2019. ***Wind variability over the northern Indian Ocean during the past 4 million years–Insights from coarse aeolian dust (IODP exp. 359, site U1467, Maldives)****. [J]. Palaeogeography, Palaeoclimatology, Palaeoecology, 536, 109371.*

摘要:来自 IODP 359 计划 U1467 孔（马尔代夫）的碳酸盐岩沉积物记录了北印度洋过去 4 Ma 的粉尘传输。颗粒大小可作为粉尘通量和季风传输能力的指标。在中、粗粉砂粒径范围内粉尘的携带与长距离传输与阿拉伯夏马尔风和对流风暴密切相关。研究结果表明在 4-3.3 Ma 间粉尘通量增加且粒径增大，与印度尼西亚海道关闭及南亚季风强度相对应。在 3.3-1.6 Ma 时间段内，粉尘通量并无明显变化趋势，而季风传输能力在降低。1.6 Ma 至今，尤其在过去 500 kyr，粉尘通量变化范围增大并呈增强趋势。1.2-0.5 Ma 间季风的传输能力增强，之后有微弱降低。频谱分析表明偏心率控制的轨道尺度变化，整个 4 Ma 间均是显著的 400 kyr 周期，在 2.0-1.3 Ma 和 1 Ma 至今是显著的 100 kyr 周期。风尘传输能力和粉尘传输量中，前者的高频循环（斜率与岁差）更为显著。数据表明相较于粉尘源区干旱变化，更倾向于由传输机制的变化引起的马尔代夫沉积物中粗颗粒的含量变化。

ABSTRACT：The lithogenic fraction of carbonate drift sediments from IODP Exp. 359 Site U1467 (Maldives) provides a unique record of atmospheric dust transport over the northern Indian Ocean during the past 4 Myr. Grain-size data provide proxies for dust flux (controlled by source area aridity) as well as wind transport capacity (wind speed). Entrainment and long-range transport of dust in the medium to coarse silt size range is linked to the strength of the Arabian Shamal winds and the occurrence of convective storms which prolong dust transport. Dust flux and the size of dust particles increased between 4.0 and 3.3 Ma, corresponding to the closure of the Indonesian seaway and the intensification of the South Asian Monsoon. There is no clear trend in dust flux between 3.3 and 1.6 Ma, whereas wind transport capacity decreased. Between 1.6 Ma and the Recent, dust flux increased and shows higher variability, especially during the last 500 kyr. Transport capacity increased between 1.2 and 0.5 Ma and slightly decreased since then. Frequency

analysis shows that dust transport varies on orbital timescales, with eccentricity control being the most prominent (400 kyr throughout the record, 100 kyr between 2.0 and 1.3 Ma, and since 1.0 Ma). Higher frequency cycles (obliquity and precession) are more pronounced in wind transport capacity than in the amount of dust. This indicates that the amount of coarse dust in sediments from the Maldives as a far-field site is more prone to changes in transport mechanisms than to changes in dust source-area aridity.

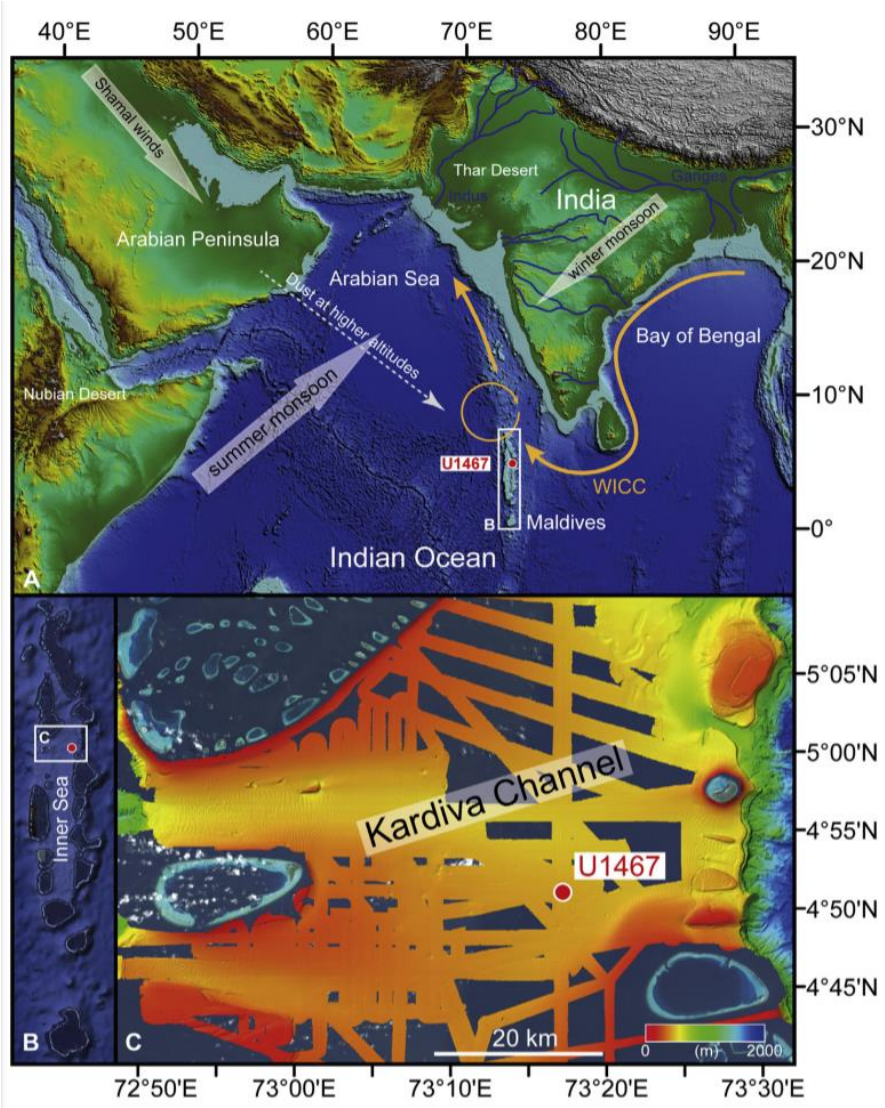

Figure 1. **a**, **b**, Location of the study site in the Indian Ocean; WICC: West India Coastal Current during northern hemisphere winter months (after Shetye, 1998); **c**, Multibeam bathymetry of the Maldives' Inner Sea surrounding the IODP expedition 359 drilling site U1467. Red dot marks position of IODP site U1467. (For interpretation of the references to colour in this figure legend, the reader is referred to the Web version of this article.)

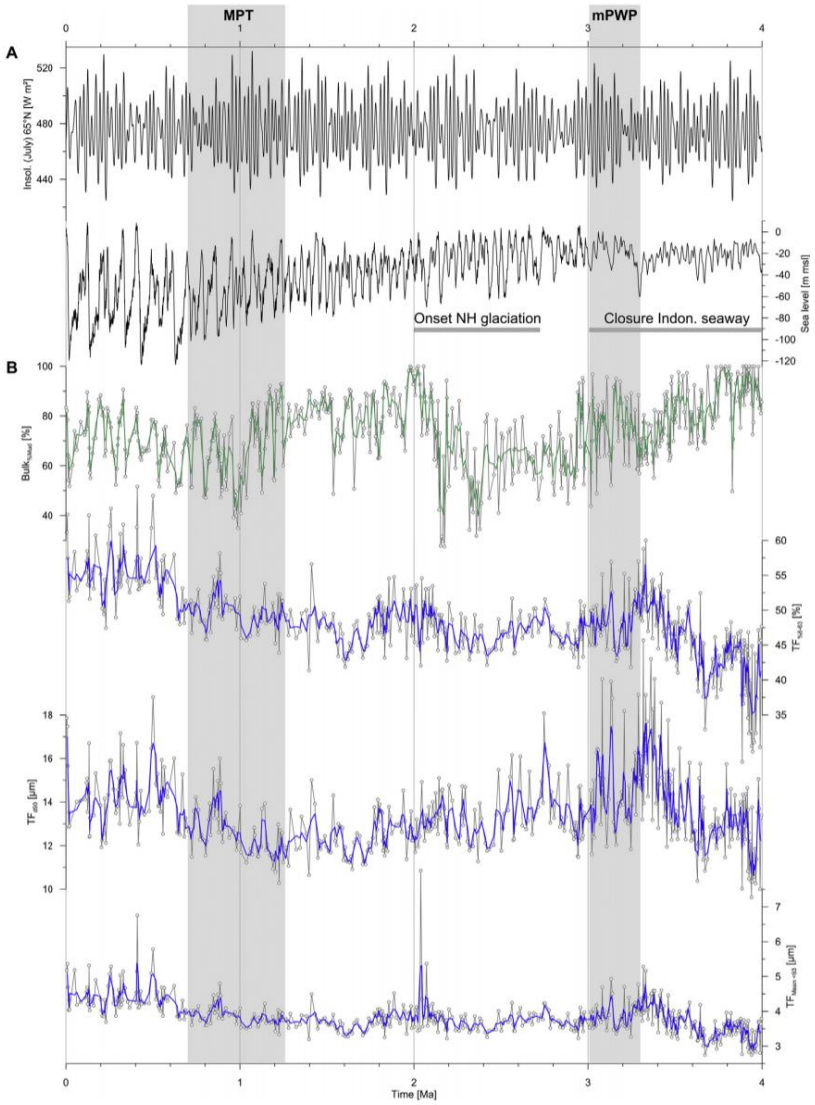

Figure 2. **a**, Summer insolation for 65 ºN and sea-level data of Miller et al. (2005); **b**, Results of grain-size analyses of the bulk and the terrigenous sediment fraction of Site U1467 sediments: Percentage of bulk mud (Bulk%mud); percentage of terrigenous particles in the size range 8-63 µm ($TF_{\%8\text{-}63}$); size of largest terrigenous particles (TF_{d90}); mean grain size of the terrigenous fraction < 63 µm (TFMean < 63). Main global climate events are indicated for orientation: Middle Pleistocene Transition (MPT; 1.25–0.75 Ma; Clark et al., 2006); mid Pliocene warm period (mPWP; 3.3–3.0 Ma; Haywood et al., 2016); onset of extensive northern Hemisphere glaciation (since 2.7 Ma; Shackleton et al., 1984; Haug et al., 1999); closure of Indonesian seaway (4.0–3.0 Ma; Cane and Molnar, 2001).

4. 西南日本现代河流沉积物 Sr-Nd-Pb 同位素系统---对西北太平洋沉积物源的指示

翻译人：刘伟 inewway@163.com

Yu Saitoh, Masaharu Tanimizu, Tsuyoshi Ishikawa. ***Sr-Nd-Pb isotope systematics of fine sediments from the modern rivers in SWJapan: Implications for sediment provenance of the Northwest Pacific*** *[J].* ***Journal of Asian Earth Sciences****, 2020, doi.org/10.1016/j.jaesx.2020.100029*

摘要：本文以日本西南部 48 条河流的沉积物为研究对象，研究了沉积物的 Sr-Nd-Pb 同位素组成，为西北太平洋地区深海沉积物的综合物源分析提供了参考资料。Sr-Nd-Pb 同位素比值是沉积物来源的可靠指标。虽然中国干旱地区的细粒沉积物（以亚洲粉尘源区闻名）的同位素资料是丰富的，但日本西南部的类似资料则是稀少的，尽管日本西南部由于其构造活动是西北太平洋的主要沉积物来源。日本河流细沉积物样品 Sr-Nd-Pb 同位素比值差异较大（$^{87}Sr/^{86}Sr$, 0.707–0.724; $^{143}Nd/^{144}Nd$, 0.5120–0.5129; $^{206}Pb/^{204}Pb$, 18.16–18.89; $^{207}Pb/^{204}Pb$, 15.55–15.66; $^{206}Pb/^{204}Pb$, 38.13–39.09)，这些变化明显依赖于各河流流域的主要地质条件。这些结果表明同位素比值可以有效地判别沉积物的来源。物源为第四纪火山岩的沉积物有最低的 $^{87}Sr/^{86}Sr$ 和 Pb 同位素比值以及最高的 $^{143}Nd/^{144}Nd$ 比值，而物源为增生沉积岩的沉积物主要表现为高的 $^{87}Sr/^{86}Sr$ 和 Pb 同位素比值以及低的 $^{143}Nd/^{144}Nd$ 比值，但他们的特定值取决于岩石的年龄和地理位置。物源来源于白垩纪花岗岩和变质岩的沉积物的同位素组成也很独特。日本河流沉积物与西北太平洋海底沉积物同位素比值的对比，表明黑潮向西北太平洋输沙的重要性。

ABSTRACT: As reference data for comprehensive provenance analyses of deep-sea sediments in the Northwest Pacific region, we present Sr-Nd-Pb isotopic compositions of fine sediments sampled from 48 rivers in southwest Japan. Sr-Nd-Pb isotope ratios are reliable indicators of sediment sources. Although isotopic data of fine sediments in Chinese arid regions, known to be Asian dust sources, are abundant, comparable data from southwest Japan are scarce, even though southwest Japan, owing to its tectonic activity, is a major sediment source to the Northwest Pacific. Sr-Nd-Pb isotope ratios of our riverine fine sediment samples vary greatly (87Sr/86Sr, 0.707–0.724; 143Nd/144Nd, 0.5120–0.5129; 206Pb/204Pb, 18.16–18.89; 207Pb/204Pb, 15.55–15.66;

and 206Pb/204Pb, 38.13–39.09), and these variations are clearly dependent on the principal geology of each river's watershed. These results indicate that these isotope ratios can be effectively used to discriminate the geological sources of the sediments. Sediments from watersheds dominated by Quaternary volcanic rocks have the lowest 87Sr/86Sr and Pb isotope ratios and the highest 143Nd/144Nd ratios, whereas sediments from watersheds dominated by accretionary sedimentary rocks generally have high 87Sr/86Sr and Pb isotope ratios and low 143Nd/144Nd ratios, but their specific values vary depending on the age and geographic location of the rocks. The isotope compositions of sediments from watersheds with exposed Cretaceous granitic and metamorphic rocks are also distinctive. Comparison between the isotope ratios of Japanese river sediments and the Northwest Pacific seafloor sediments suggests the importance of sediment transport by the Kuroshio Current to the Northwest Pacific.

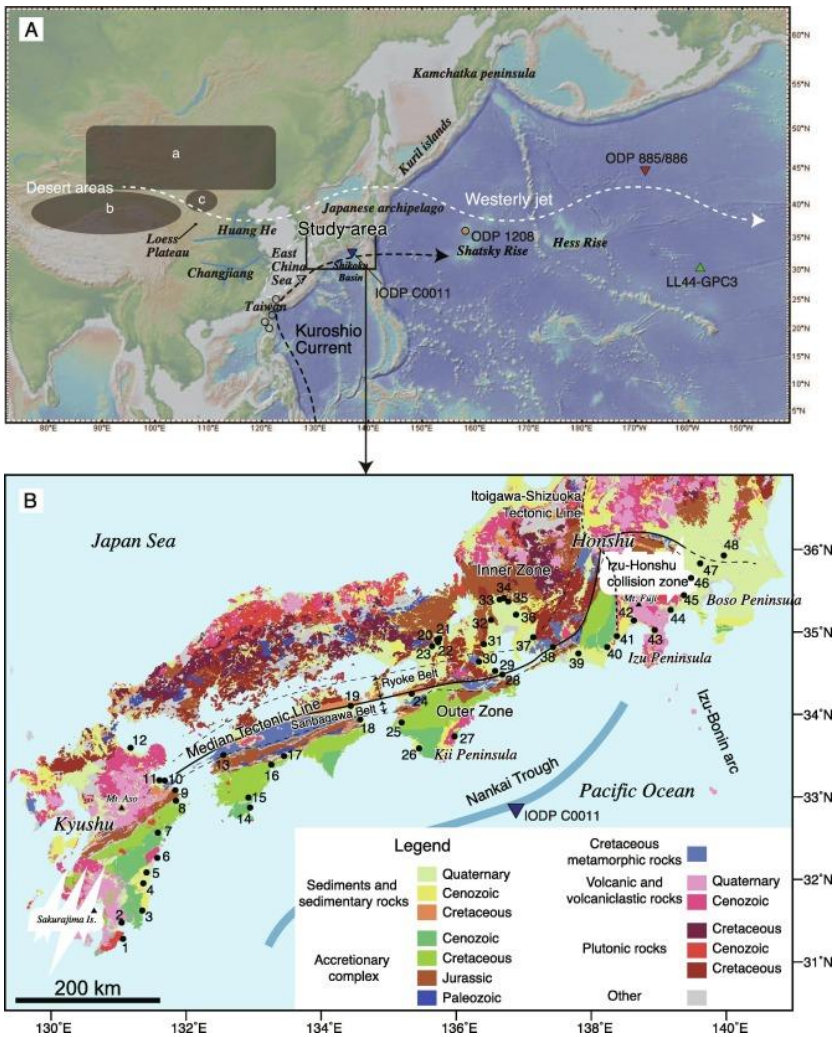

Figure 1. A. Location of the study area, drilling sites of the ocean-floor sediments compared with the

results of this study, possible sources of Asian dust (desert areas a: on the northern boundary of China, b: on the northern margin of Tibetan Plateau, and c: on the Ordos Plateau, and the Loess Plateau), and fluvial sources in relation to the path ways of the westerly jet and the Kuroshio Current. B. River sediment sampling sites and the distribution of geological units in southwest Japan (modified after Geological Survey of Japan, AIST, 2015).

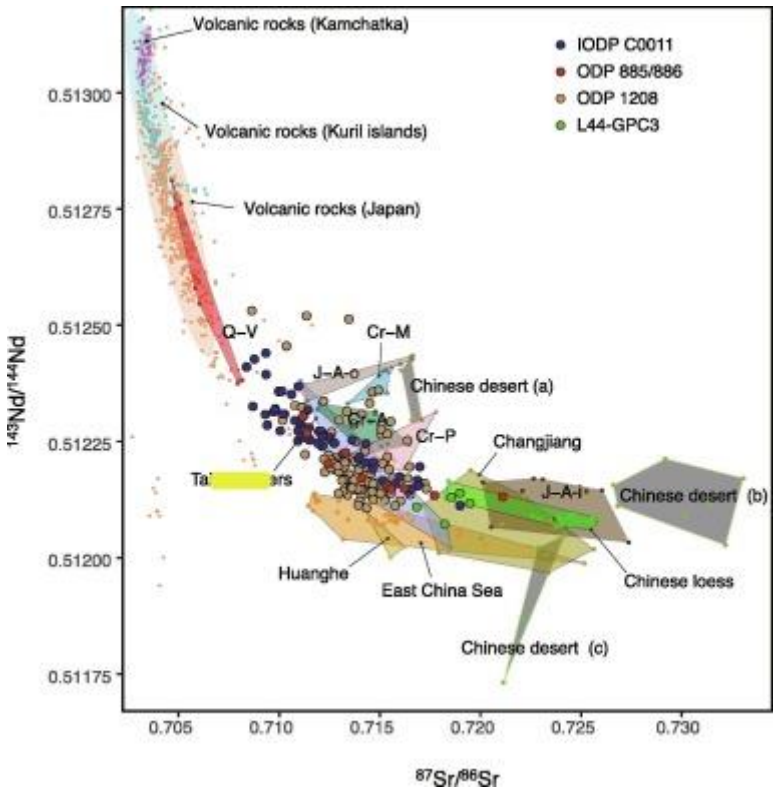

Figure 2. Comparison of Sr–Nd isotope ratios of deep-sea sediments in the North Pacific (L44-GPC3; Pettke et al., 2000; ODP 885/886: Pettke et al., 2002; ODP1208: Zhang et al., 2016; IODP C0011: Saitoh et al., 2015) with those of sediments in possible sources, Chinese loess (Sun, 2005), Chinese desert (Chen et al., 2007), Volcanic rocks along the western margin of the North Pacific (GEOROC, http://georoc.mpch-mainz.gwdg.de/georoc/), Taiwanese rivers (Zheng et al. 2016), Changjiang (Yang et al., 2007, Meng et al., 2008), East China Sea (Dou et al., 2012, Saitoh et al., 2015), and rivers in southwest Japan dominated by the 6 major geological units (J-A-i; Jurassic accretionary complex in the inner belt, J-A-o; Jurassic accretionary complex in the Outer Zone, Cr-A; Cretaceous accretionary complex, Cr-M; Cretaceous metamorphic rocks, Cr-P; Cretaceous plutonic rocks, and Q-V; Quaternary volcanic rocks).

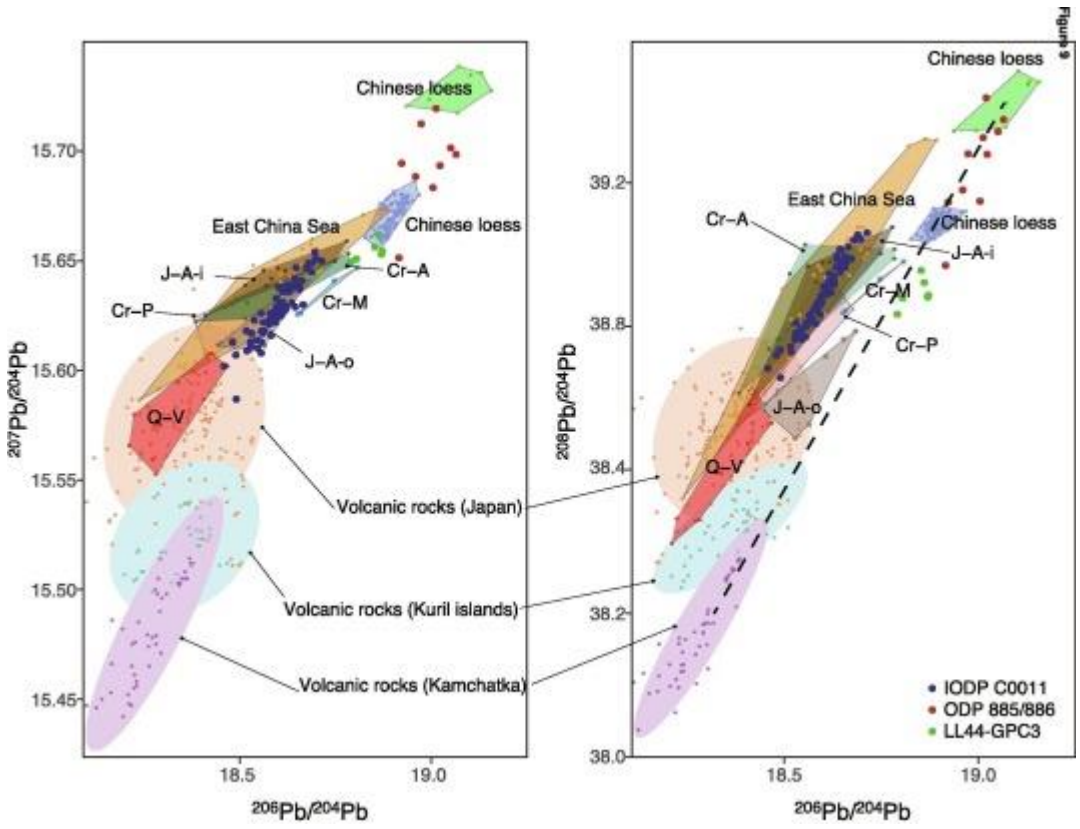

Figure 3. Comparison of Pb isotope ratios of deep-sea sediments in the North Pacific (L44-GPC3; Pettke et al., 2000; ODP 885/886: Pettke et al., 2002; ODP1208: Zhang et al., 2016; IODP C0011: Saitoh et al., 2015) with those of sediments in the possible sources, Chinese loess (Sun and Zhu, 2010, green; Jones et al., 2000, violet), volcanic rocks along the western margin of the North Pacific (GEOROC, http://georoc.mpch-mainz.gwdg.de/georoc/), East China Sea (Bentahila et al., 2008,; Saitoh et al., 2015), and rivers in southwest Japan dominated by the 6 major geological units (J-A-i; Jurassic accretionary complex in the inner belt, J-A-o; Jurassic accretionary complex in the Outer Zone, Cr-A; Cretaceous accretionary complex, Cr-M; Cretaceous metamorphic rocks, Cr-P; Cretaceous plutonic rocks, and Q-V; Quaternary volcanic rocks). Isotope ratios of LL44-GPC3, ODP 885/886, IODP C0011 and East China Sea sediments have been corrected against NIST SRM 981 values ($^{206}Pb/^{204}Pb$ = 16.9308; $^{207}Pb/^{204}Pb$ = 15.4839; $^{208}Pb/^{204}Pb$ = 36.6743; Tanimizu and Ishikawa, 2006).

5. 印度夏季风在轨道-千年尺度上的变率

翻译人：杨会会 11849590@mail.sustech.edu.cn

Kathayat G, Cheng H, Ashish Sinha et al. ***Indian monsoon variability on millennial-orbital timescales[J].Scientific Reports,*** *2016,6:24374*

摘要：印度夏季风(ISM)对生活在该地区的数十亿人来说至关重要。然而，在轨道-千年尺度上，关于 ISM 的主要驱动力仍然存在重大争论。本文中我们根据印度北部 Bittoo 洞穴的石笋氧同位素($\delta^{18}O$)数据，重建了过去 280 ka 的 ISM 变率。我们发现印度北部的石笋 $\delta^{18}O$ 记录和中国东亚季风主导区的石笋 $\delta^{18}O$ 记录具有很强的一致性，说明这两个亚洲季风子系统都对北半球夏季日照(NHSI)的变化表现出耦合响应，且没有显著的时间滞后，这也支持热带-亚热带季风变率直接由岁差周期引导的 NHSI 变化所驱动。根据末次冰期期间印度北部记录与南极冰芯和南印度洋洋表温度记录的对比表明，南半球气候过程在轨道-千年尺度上并不主导印度夏季风的变化。

ABSTRACT: The Indian summer monsoon (ISM) monsoon is critical to billions of people living in the region. Yet, significant debates remain on primary ISM drivers on millennial-orbital timescales. Here, we use speleothem oxygen isotope ($\delta^{18}O$) data from Bittoo cave, Northern India to reconstruct ISM variability over the past 280,000 years. We find strong coherence between North Indian and Chinese speleothem $\delta^{18}O$ records from the East Asian monsoon domain, suggesting that both Asian monsoon subsystems exhibit a coupled response to changes in Northern Hemisphere summer insolation (NHSI) without significant temporal lags, supporting the view that the tropical-subtropical monsoon variability is driven directly by precession-induced changes in NHSI. Comparisons of the North Indian record with both Antarctic ice core and sea-surface temperature records from the southern Indian Ocean over the last glacial period do not suggest a dominant role of Southern Hemisphere climate processes in regulating the ISM variability on millennial-orbital timescales.

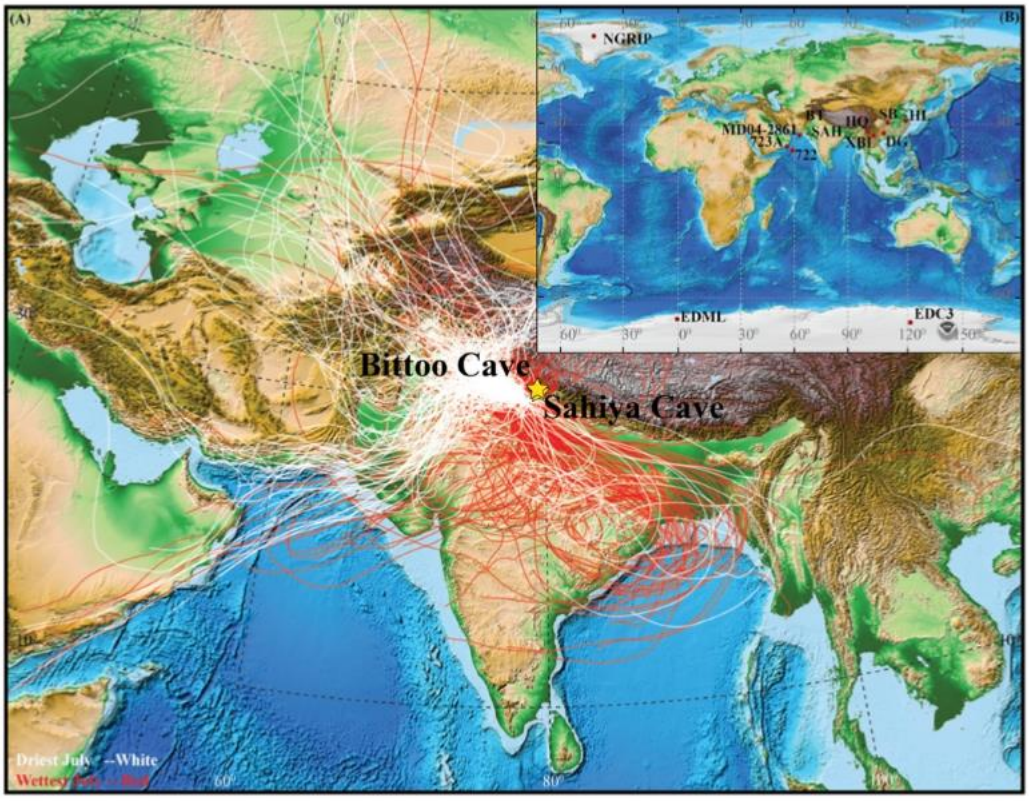

Figure 1. Location map. (A) Schematic map ETOPO1[1] (Global Relief Model, NOAA http://www.ngdc.noaa.gov/mgg/image/color_etopo1_ice_low.jpg,Computerized digital images and associated databases are available from the National Centers for Environmental Information, National Oceanic and Atmospheric Administration, U.S. Department of Commerce, http://www.ngdc.noaa.gov/.) showing the Bittoo (BT) and Sahiya (SAH) caves (yellow stars) in North India and low-level air parcel trajectories computed from the HYSPLIT model[2]. (B) Inset panel shows locations of climate records used for comparison (red dots): Greenland ice core (NGRIP), Antarctic ice cores (EDML/EDC), Arabian Sea cores (722/MD04-2861/723A), Hulu (HL), Xiaobailong (XBL), Tianmen (TM), Dongge (DG) and Sanbao (SB) East Asian monsoon (EAM) records from Chinese speleothems, and the Heqing (HQ) lake record.

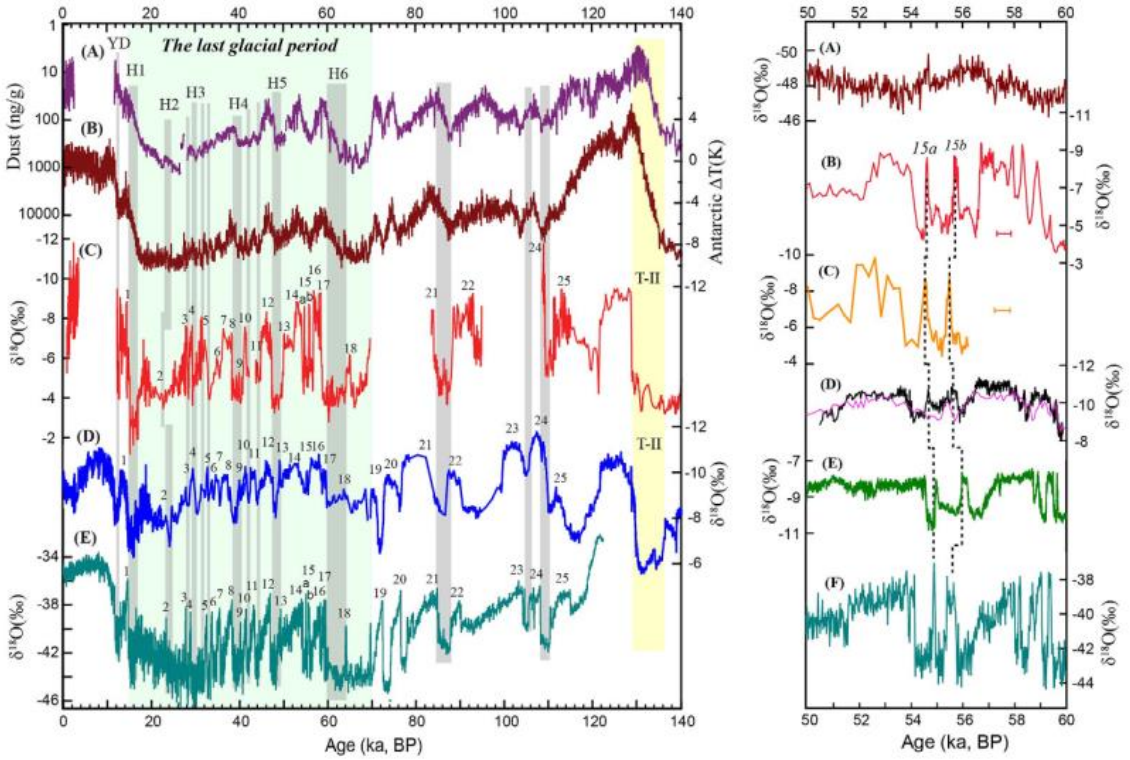

Figure 2. Comparison of climate events in ISM and EAM records over the last 140 ka. Left panel: (A) and (B) are dust[41] and temperature[30] records from Antarctic ice-core EDC, respectively. (C) Northern India $\delta^{18}O$ record. (D) EAM $\delta^{18}O$ record25. (E) Greenland NGRIP ice-core $\delta^{18}O$ record[22]. Vertical grey bars indicate weak ISM events and their correlations to weak EAM events, cold events in Greenland, and higher temperature and less dust loading in Antarctica. The yellow bar shows glacial termination T-II. Numbers depict the Indian (C), Chinese (D) and Greenland (E) Interstadials, respectively. These millennial-scale variations are synchronous within age uncertainties. Light-green shading marks the last glacial period. The synchronicities of MIS 3 and MIS 5e between the ISM and EAM demonstrate the in-phase variability of the two monsoon systems on the orbital timescale. Right panel: (A) Antarctic ice core EDML $\delta^{18}O$ record[42]. The $\delta^{18}O$ scale is reversed as compared with speleothem records. (B,C) ISM records from Bittoo cave stalagmites BT-2 (red) and BT-1 (orange). Error bars depict typical 230T dating errors (2σ). (D) EAM record from Chinese speleothem records (Wulu record in black[31] and Hulu record in purple[25]). (E) The central Europe temperature variation inferred from speleothem records[32]. (F) Greenland NGRIP $\delta^{18}O$ ice-core record[22]. The striking similarity/diff erence of the ISM variability with/from Greenland/Antarctic records implies a dominant NH rather than SH control on ISM dynamics.

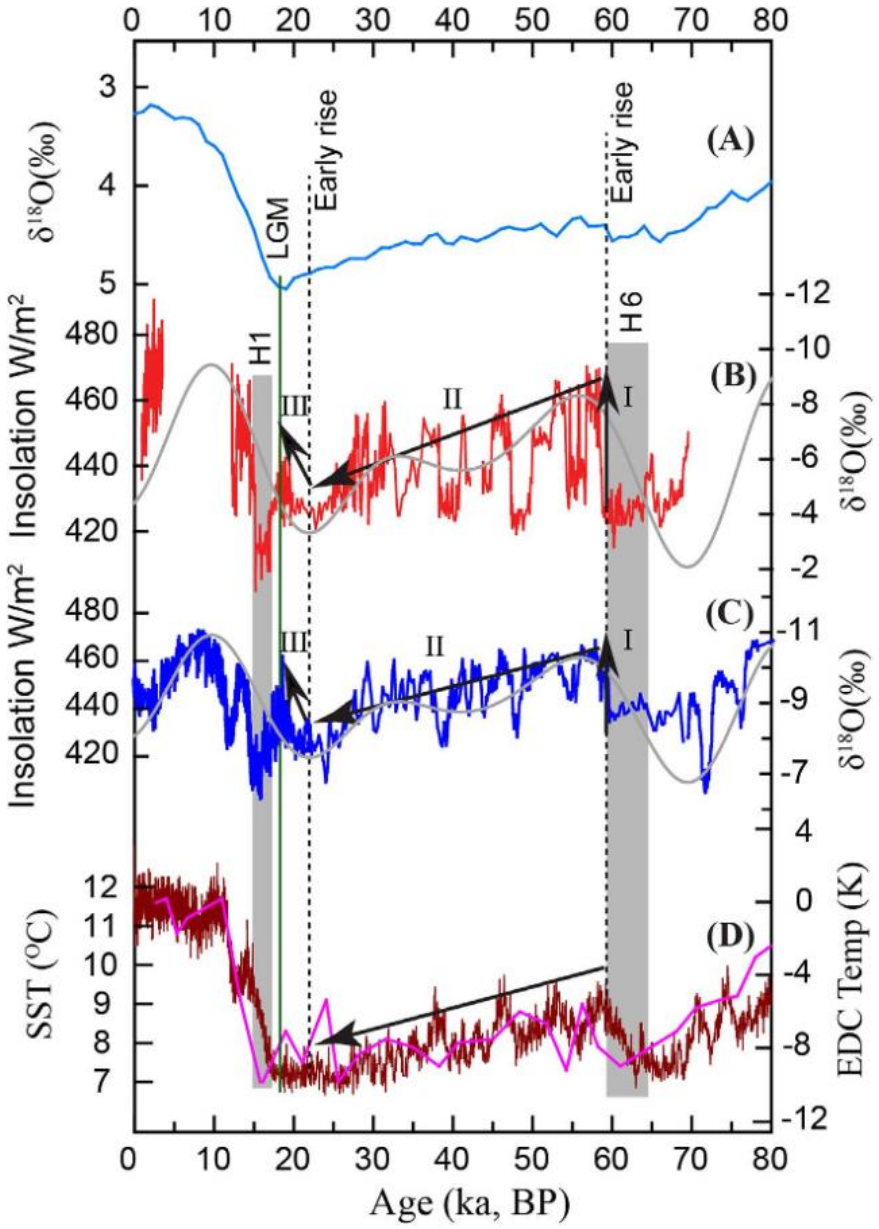

Figure 3. Early ISM increases prior to the LGM during the last glacial period. (A) Benthic stack $\delta^{18}O$ record43. (B) North India record (red) and July 21 insolation 65 ℕ[40] (grey curve). (C) EAM record[25] (blue) and July 21 insolation 65 ℕ[40] (grey curve). (D) Antarctic temperature record from ice core EDC[30] (brown) and southern Indian Ocean SST[29] (purple). The vertical grey bars depict Heinrich events 1 and 6. Arrow-I marks the abrupt shift of both ISM and EAM at ~60 ka BP when Antarctic temperature reached a maximum about 40 ka prior to the LGM. Arrow-II depicts the ISM and EAM decline concurrently with temperature decreases of both Antarctica and southern Indian Ocean (arrow in D) rather than their temperature increases. Arrow-III indicates another early ISM and EAM rise at ~22 ka BP, about 2.5 ka prior to the LGM and about 3 ka after Antarctic temperature reached the minimum at ~25 ka BP. Both early monsoon rises appear to have coincided with NHSI rise rather than with an Antarctic temperature cooling (D), thus providing an alternative explanation.

6. 南极洲东部恩德比盆地的地壳结构

翻译人：曹伟 11930854@mail.sustech.edu.cn

Davis J K , Lawver L A , Norton I O , et al. ***The crustal structure of the Enderby Basin, East Antarctica****[J].* ***Marine Geophysical Research****, 2018. DOI：10.1007/s11001-018-9356-5*

摘要：南极洲东部恩德比盆地的被动边缘和洋壳保存了东冈瓦纳大陆裂解的记录。通过使用一系列公开的地球物理数据，我们分析并描述了盆地的地壳形态。根据地球物理观察结果，我们将恩德比盆地划分为三个不同的形态域。东部区域火山形态最为明显，有大量的向海倾斜反射层和异常厚的洋壳，这些特征显示了 Kerguelen 热点对区域内大陆裂解的早期影响。中部区域的特征是两个形态各异的洋壳区域被一个高振幅磁异常分隔开来。地球物理观测表明，该磁异常的内测基底是由薄的、高低不平、结构性较差的原始洋壳组成，其形态类似于在超慢速/慢速扩张洋中脊形成的洋壳。在该异常的外侧，洋壳结构性较好，厚度正常。我们对观测到的海洋地壳结构变化提供了三种非排他性的解释：（1）大陆裂解初期，熔岩的最初产生量较低，而随着地幔逐渐减压，导致熔岩产生量和洋壳厚度逐渐增加；（2）由于扩张速率较低，熔岩最初产量较低，而随着扩张速率的变化，熔岩产量增加；（3）扩张脊形状的变化导致更有效率的海底扩张，同时增加了熔岩产量。恩德比盆地西部以丰富的断裂带和异常薄的洋壳为特征，我们认为这些特征是大陆裂谷作用于域内伸展最初倾斜方向的几何结果。综合观测结果可知，东冈瓦纳大陆的裂解是高度可变的，在地壳变形和海底扩张过程中存在显著的走向差异。

ABSTRACT：The passive margin and ocean crust of the Enderby Basin, East Antarctica preserves a record of the breakup of East Gondwana. Using a suite of public domain geophysical data, we have examined and described the crustal morphology of the basin. Based on our geophysical observations, we divide the Enderby Basin into three distinct morphologic domains. The Eastern Domain demonstrates the most volcanic morphology of the basin, with abundant seaward dipping reflector packages and anomalously thick oceanic crust. These features suggest an early influence by the Kerguelen Hotspot on continental breakup within the domain. The Central Domain is characterized by two regions of oceanic crust of varying morphology segregated by a high amplitude magnetic anomaly. Geophysical observations suggest that the

basement directly inboard of this magnetic anomaly is composed of thin, rugged, and poorly structured, proto-oceanic crust, similar in morphology to oceanic crust formed at ultraslow/slow mid-ocean ridged. Outboard of this anomaly, oceanic crust appears to be well-structured and of normal thickness. We offer three, non-exclusive, explanations for the observed change in ocean crustal structure: (1) melt production was initially low at the time of continental breakup, and the progressive decompression of the mantle led to a gradual increase in melt production and ocean crust thickness, (2) melt production was initially low to due lower extension rates and that melt production increased following a change in spreading rate, (3) a change in spreading ridge geometry led to more effective seafloor spreading rate and concurrent increase in melt production. The Western Domain of the Enderby Basin is characterized by abundant fracture zones and anomalously thin oceanic crust. We believe these features arose as a geometric consequence of the originally oblique orientation of continental rifting relative to the extension direction within the domain. Together these observations suggest that the breakup of East Gondwana was highly variable, with notable alongstrike differences in crustal deformation and seafloor spreading processes.

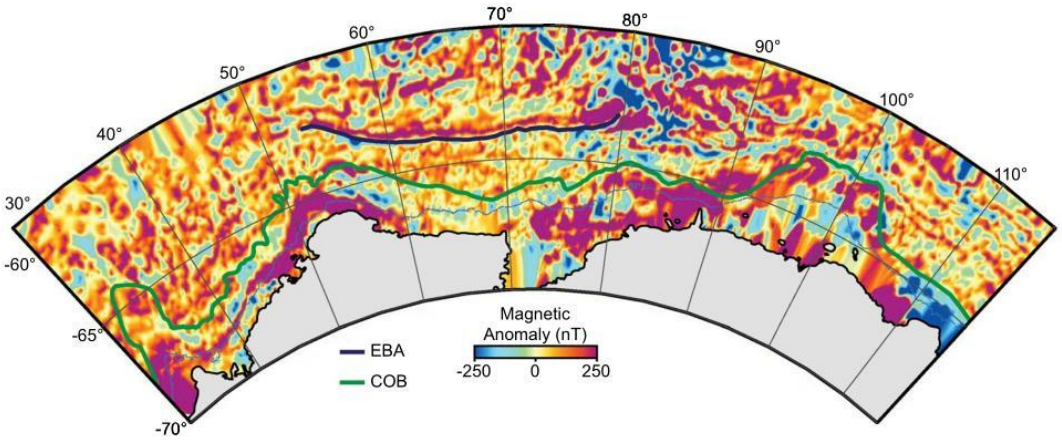

Figure 1. Antarctica Digital Magnetic Anomaly Project (ADMAP) magnetic anomaly compilation (Golynsky et al. 2013), the Enderby Basin anomaly (EBA), and the continent–ocean boundary (COB) proposed by this study

7. 石笋中与永冻土相关的沉积间断：评估重建碳循环动力学的潜力

翻译人：郑威 11930589@mail.sustech.edu.cn

Lechleitner F A, Mason A J, Breitenbach S F M, et al. ***Permafrost-related hiatuses in stalagmites: Evaluating the potential for reconstruction of carbon cycle dynamics****[J]. **Quaternary Geochronology**, 2020, 56: 101037.*

摘要：永冻土广泛存在于北半球高纬地区，以冻土有机质形式储存了大量的碳。永冻土地区对人为气候变化的响应任不确定，部分原因是缺少它们对过去全球气候变化响应的信息。在这里，我们测试了西伯利亚两个洞穴的石笋作为新的高精度定年和高度当地化过去永冻土碳循环动力学记录档案的使用性。在冰期-间冰期尺度，这些地方石笋的生长受控于洞穴是否存在上覆永冻土。我们以三个石笋中两个后续生长期（间冰期）和末次冰期恢复生长后的阶段之间的过渡层为研究目标，因为这里记录了冻土区地表和洞穴之间解冻过程相关的地化足迹。我们应用了多指标方法包括碳同位素（$\delta^{13}C$, ^{14}C）和微量元素，结合岩相学分析和高分辨率U-Th年代框架。我们的数据指示了过度层复杂的生长模式和可能的石笋表面微生物繁殖期。高分辨率U-Th年龄证实了过渡层不是一个单一的长时间生长间断，而是一个极度缓慢或者偶发生长的时期，可能是在“失落在冰期的”间冰期期间。但是，我们没有发现与永冻土退化和相关当地碳循环动力学相关的地化信号的实锤，这可能是由于石笋档案对高频过程的敏感度不足或测量分辨率不足。

ABSTRACT：Permafrost is widely present throughout the Northern Hemisphere high latitudes, and stores large amounts of carbon in the form of frozen soil organic matter. The response of permafrost regions to anthropogenic climate change remains uncertain, in part because of a lack of information on their response to past changes in global climate. Here we test the use of stalagmites from two caves in Siberia as a novel, precisely dated, and highly localised archive of past permafrost carbon cycle dynamics. Stalagmite growth at these sites is controlled by the presence/absence of permafrost above the cave over glacial-interglacial time scales. We target the transition layer between two subsequent growth phases (interglacials) and the interval directly following growth resumption after the last glacial in three stalagmites, as this is where a geochemical imprint of thaw-related processes in the frozen zone between surface and cave would

be recorded. We apply a multi-proxy approach including carbon isotopes ($\delta^{13}C$ and ^{14}C) and trace element concentrations, combined with petrographic analyses and high-resolution U-Th chronology. Our dataset indicates complex growth patterns and possible intervals of microbial colonisation of the stalagmite surface in the transition layers. High-resolution U-Th ages confirm that the transition layer is not a single, long growth hiatus, but rather a period of extremely slow or episodic growth phases, possibly during "skipped" interglacials. However, we find no conclusive evidence for a geochemical signature related to permafrost degradation and related local carbon cycle dynamics, which might be related to insufficient sensitivity of the archive for high-frequency processes and/or insufficient measurement resolution.

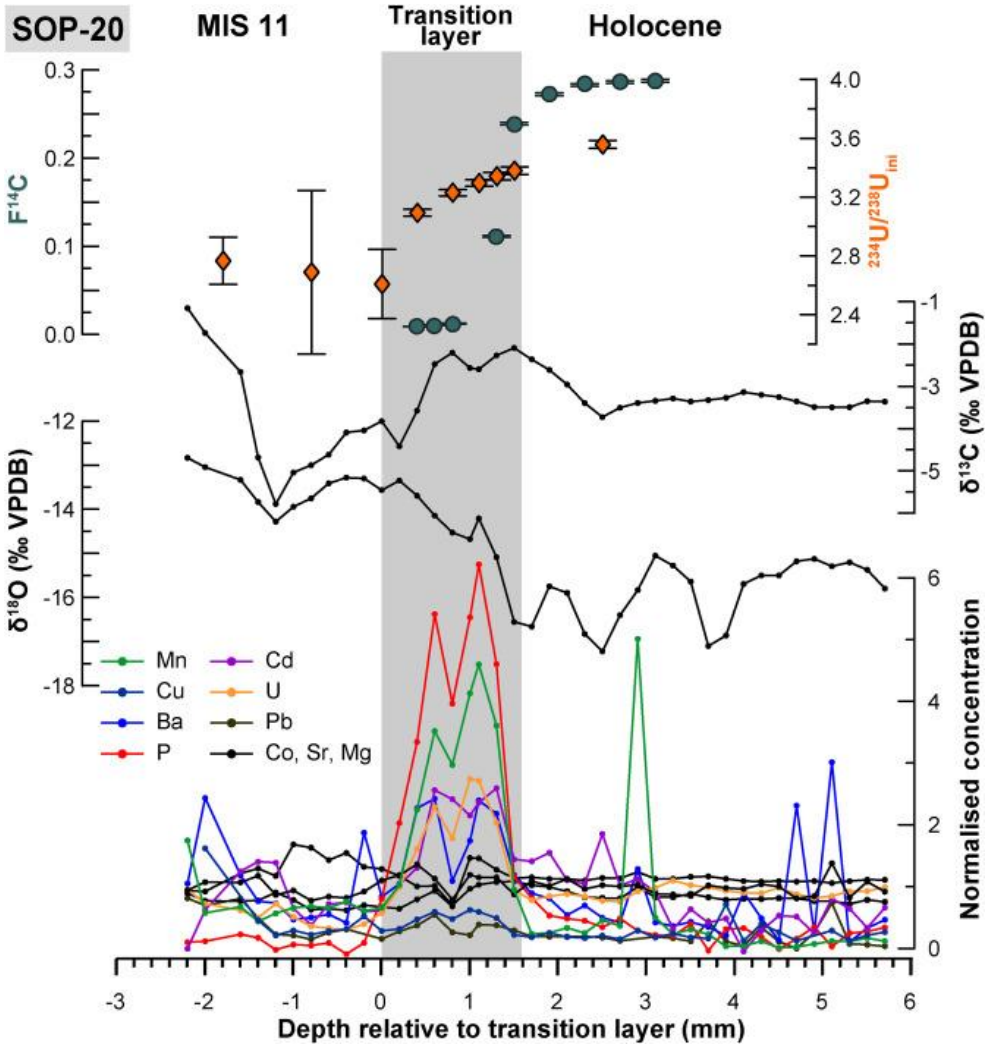

Figure 1. Results from geochemical analysis on stalagmite SOP-20. To ease intercomparison between the stalagmites, the measurement depth is normalised to the beginning of the transition layer (grey bar), defined as the start of increase in Mn concentrations. From top: $F^{14}C$, $^{234}U/^{238}U_{ini}$, $\delta^{13}C$, $\delta^{18}O$, and trace element concentrations (normalised against their average value).

8. 磁通量瓣面拉伸导致最近磁北极加速向西伯利亚移动

翻译人：柳加波

Livermore, P.W., Finlay, C.C. & Bayliff, M. ***Recent north magnetic pole acceleration towards Siberia caused by flux lobe elongation.*** *Nat. Geosci. (2020).*

摘要：磁北极是地球地磁场垂直向下的位置。磁北极的漂移一直是科学研究中令人着迷的一个主题。自从 1831 年首次在加拿大北极地区实地观测以来，磁北极一路向西伯利亚漂移。在 1990 年至 2005 年期间，磁北极的漂移速度由 0-15 $km\ yr^{-1}$ 加速到现今的 50-60 $km\ yr^{-1}$。在 2017 年 10 月下旬，磁北极越过国际日期变更线，距离地球地理北极仅 390 km，然后继续一路向南。我们发现，在过去二十年中，磁北极的位置在很大程度上是由加拿大和西伯利亚下方核幔边界上两个大的磁通量负值瓣面决定的。局部模型显示，加拿大磁通量瓣面的拉伸，可能是由 1970 年至 1999 年间岩心流动模式变动引起的。从而削弱了加拿大磁通量瓣面在地表的信号，导致磁北极加速向西伯利亚移动。捕捉到这一过程的一系列简单模型表明，在未来十年中，磁北极将沿着当前轨迹，继续向西伯利亚再前进 390-660 公里。

ABSTRACT： The wandering of Earth's north magnetic pole, the location where the magnetic field points vertically downwards, has long been a topic of scientific fascination. Since the first in situ measurements in 1831 of its location in the Canadian arctic, the pole has drifted inexorably towards Siberia, accelerating between 1990 and 2005 from its historic speed of 0–15 $km\ yr^{-1}$ to its present speed of 50–60 $km\ yr^{-1}$. In late October 2017 the north magnetic pole crossed the international date line, passing within 390 km of the geographic pole, and is now moving southwards. Here we show that over the last two decades the position of the north magnetic pole has been largely determined by two large-scale lobes of negative magnetic flux on the core–mantle boundary under Canada and Siberia. Localized modelling shows that elongation of the Canadian lobe, probably caused by an alteration in the pattern of core flow between 1970 and 1999, substantially weakened its signature on Earth's surface, causing the pole to accelerate towards Siberia. A range of simple models that capture this process indicate that over the next decade the north magnetic pole will continue on its current trajectory, travelling a further 390–660 km towards Siberia.

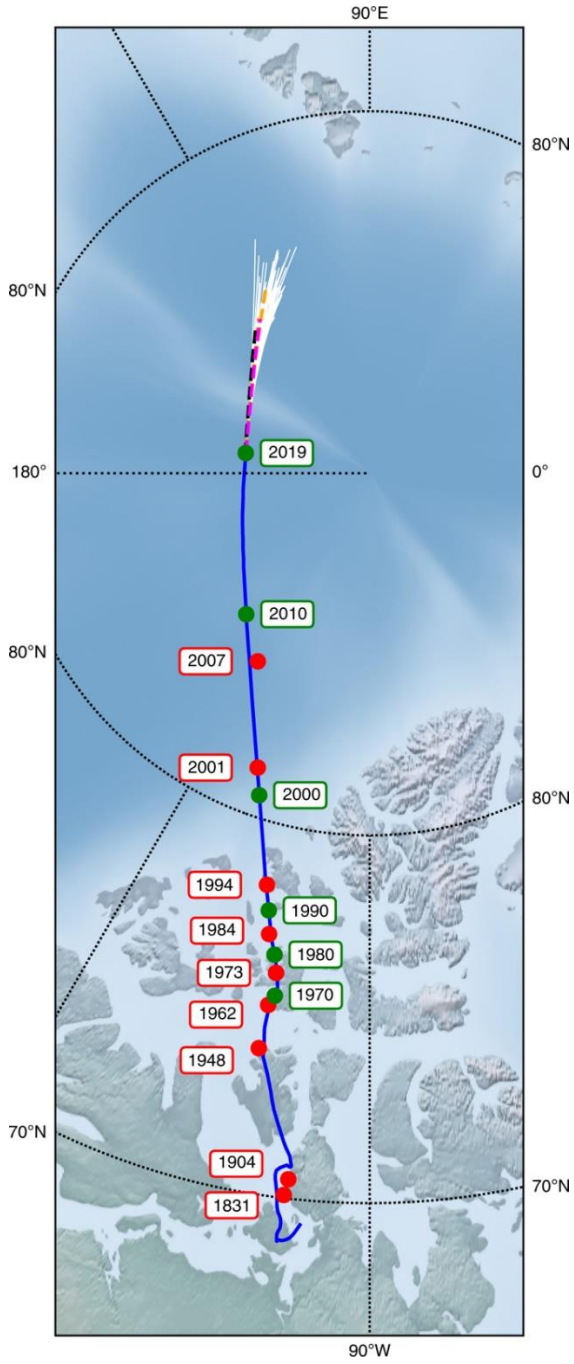

Figure 1. Historical movement and predicted future path of the north magnetic pole in stereographic projection. Solid blue shows the pole's evolution according to the COV-OBS.x1 (1840–1999) and CHAOS-6-x8 (1999–2019) geomagnetic field models, with green circles indicating recent decadal positions; red circles mark in situ measurements (1831–2007). The international date line is shown by the dotted black line on the 180 °meridian. Predictions (Methods) 2019–2029 are linear extrapolations from the World Magnetic Model Version 2 in black, linear extrapolation from CHAOS-6-x8 in magenta, a purely diffusive model based on fitting geomagnetic secular variation over 2014–2019 in orange and frozen-flux evolution using an ensemble of large-scale flows in white.

9. 南大洋磁性矿物含量变化来源

翻译人：王敦繁

Toshitsugu, Yamazaki. ***Origin of magnetic mineral concentration variation in the Southern Ocean****[J]. Paleoceanography, 2012.*

摘要：南大洋沉积物中磁性矿物的含量在冰期显著增加，这与南极冰芯中的风尘通量变化记录相似。但是，它们造成两者之间如此联系的原因仍然未知，比如在南大洋陆源矿物的输入相比风尘输入含量十分有限。为了查明磁性矿物含量变化的来源，我们对晚更新世南印度洋沉积物的环境磁学进行了系统研究。生物来源的磁铁矿可以根据其微弱的磁相互作用和较窄的矫顽力分布识别出链状单畴磁小体的存在。我们解释了一阶反转曲线图上的无相互作用和等温剩磁(IRM)均一的低矫顽力组分代表生物成因的磁铁矿，而相互作用分量和中矫顽力组分代表陆源的磁赤铁矿。ARM 和 IRM 的比值反映了生物源和陆源的相对丰度，并揭示了生物磁铁矿是主要的磁性矿物成分。冰期随着陆源磁性矿物的增加生物磁铁矿含量也随之增加。同时拉长型磁小体含量的增加指识出缺氧环境和沉积速率增加，这说明在冰期生产力的提高。这些观测结果表明，南大洋沉积物中冰期磁性矿物含量的增加可能与铁施肥效应有关;生物磁铁矿的产生与海洋生产力的提高有关，并且海洋生产力的提高是由风尘通量的增加所推动的。

ABSTRACT: In the Southern Ocean, magnetic mineral concentration increases in glacial periods. The variation pattern closely resembles eolian dust flux records from Antarctic ice cores, but the cause of the linkage remains unclear, as the dust flux is too small for the source of terrigenous materials in the Southern Ocean. We have conducted an environmental magnetic study of late Pleistocene sediments from the south Indian Ocean to investigate the origin of the magnetic concentration changes. Biogenic magnetites can be detected using the characteristics of almost no magnetostatic interactions and narrow coercivity distribution, reflecting occurrence of single-domain magnetites in a chain. We interpret that a non-interacting component on first-order reversal curve diagrams and low-coercivity components with small dispersion from isothermal remanent magnetization (IRM) component analyses represent biogenic magnetites, and that the interacting and middle-coercivity components represent terrigenous maghemites. The ratio of anhysteretic remanent magnetization susceptibility to saturation IRM reflects relative abundance

of the biogenic and terrigenous components. It was revealed that biogenic magnetites are a dominant constituent of the magnetic minerals. In glacials, the abundance of both biogenic and terrigenous components increased with increased proportions of the latter. Increased ocean productivity in glacials is suggested from increased proportions of biogenic magnetites with elongated morphologies, indicative of less-oxic conditions, and increased sedimentation rates. These observations suggest that the increased magnetic concentration in glacials in the Southern Ocean may be explained by iron fertilization; the production of biogenic magnetites was enhanced associated with increased ocean productivity, which was fueled by increased eolian dust flux.

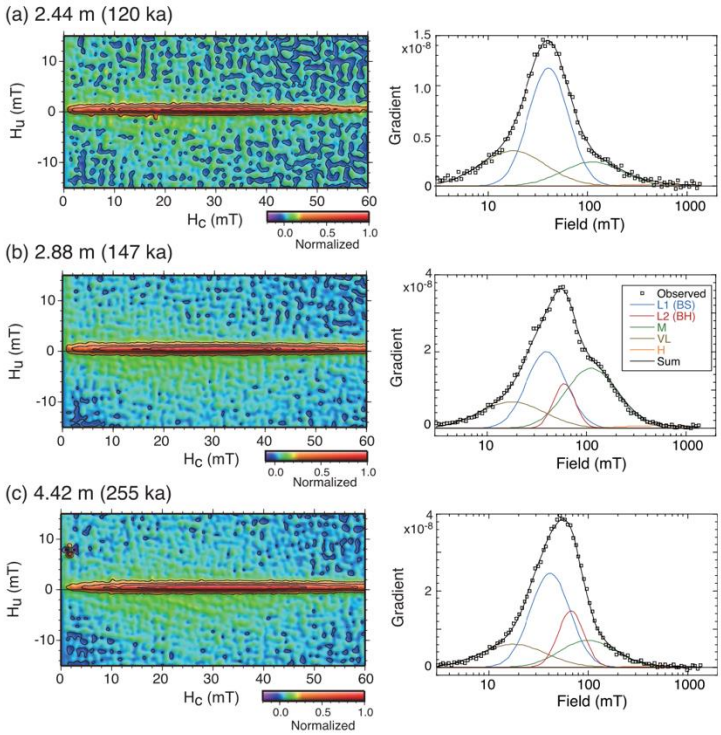

Figure 1. (a–c) Examples of high-resolution FORC diagrams (left) and corresponding IRM component analyses (right). For IRM component analyses, squares represent data points that define the gradient of the IRM acquisition curves, which can be described by the sum (black curve) of two dominant components, low-coercivity (L1, blue curve) and middle-coercivity (M, green) components, two other components, very-low-coercivity (VL, brown) and high-coercivity (H, orange) components, and occasionally another low-coercivity component with conspicuously narrow dispersion (L2, red).